DETERMINING WATER CONTENT RANGE FOR OPTIMUM SLUMP

BY

MARTIN LEWIS MONK, Jr.

A THESIS
SUBMITTED TO THE FACULTY OF

ALFRED UNIVERSITY

IN PARTIAL FULFILLMENT OF THE REQUIREMENTS
FOR THE DEGREE OF

MASTER OF SCIENCE

IN

CERAMIC ENGINEERING

ALFRED, NEW YORK

FEBRUARY, 2018

DETERMINING WATER CONTENT RANGE FOR OPTIMUM SLUMP

BY

MARTIN LEWIS MONK, Jr.

B.S. ALFRED UNIVERSITY (2015)

SIGNATURE OF AUTHOR_____

APPROVED BY_____

Dr. WILLIAM CARTY, ADVISOR

_____

Dr. S. K. SUNDARAM, ADVISORY COMMITTEE

_____

Dr. HOLLY SHULMAN, ADVISORY COMMITTEE

_____

CHAIR, ORAL THESIS DEFENSE

ACCEPTED BY_____

ALASTAIR CORMACK, INTERIM DEAN
KAZUO INAMORI SCHOOL OF ENGINEERING

ACKNOWLEDGMENTS

First and foremost, I thank Dr. William Carty, my teacher since sophomore year and the person who originally got me to study and love ceramic engineering. His knowledge, guidance and encouragement has challenged and directed my Alfred University career. He supported my attendance at two Ceramic Expo conferences and my internship at Ludowici. I am thankful for his role as my advisor on this thesis - his direction, interest, patience and scientific knowledge.

A special thank you to Hyojin Lee, who helped me further my knowledge in ceramic engineering and was always there when I needed someone to listen. My thanks to Krishna Amin who helped me schedule meetings and kept the lab and our work exciting. My sincere thanks also to Katie Decker, a wonderful boss and supervisor who provided guidance in my teaching assistant role and academic pursuits.

I am grateful to Peter Roberts, the recipient of a National Science Foundation Grant, who funded me for my first semester of graduate school. I also acknowledge and thank Southern Tier Concrete, Alfred, New York, for supplying all the raw materials for this thesis.

Finally, I would like to acknowledge my family and friends who supported me throughout my six years at Alfred University. I thank my parents, Louise Mitchell and Martin Monk, Sr. for their love and support. I am also grateful and thankful for my close friends, Nick Milliman, Greg Buisman, Kyle Luce, Eric Akalaski, Caine Cole, Duncan Martin, Nestor Agudelo, Wade Carmichael, Mike Knapp, Zachary Bagdonas and the others who crossed my path and welcomed me to Alfred University as a brother. My freshman year I arrived at Alfred alone and knew no one. I am leaving with a new family of friends and colleagues who, I know, will continue to provide guidance and love until the day I die.

TABLE OF CONTENTS

Page

Acknowledgments iii

Table of Contents iv

List of Tables vi

List of Figures vii

Abstract x

I. INTRODUCTION 1

II. LITERATURE SURVEY 4

A. General Background on Portland Cement Concrete 4

1. Concrete History 4

2. Portland Cement 4

B. Aggregate 5

C. Water-to-Cement Ratio 6

D. Specific Volume Diagram 6

E. Packing Efficiency 9

F. Water Addition Affecting Packing Efficiency 9

G. Slump Testing 10

III. EXPERIMENTAL PROCEDURE 14

A. Raw Materials 14

B. Particle Size 14

C. Design of the Experiment 16

D. Packing Density Measurement 20

1. Dry Packing Density 20

2. Rule of Mixtures (R.O.M.) 20

3. Mixing Time 20

4. Wet Packing Density 21

E. Slump Testing 22

1. Determining Water Content for Slump Test Calculations 22

2. Slump Test Procedure 22

IV. RESULTS AND DISCUSSION 24

A. Determining Packing Efficiency Using Tap Density 24

1. Dry Packing Density 24

2. Slump Test Procedure 30

3. Wet Packing Density 32
B. Slump Testing 40
C. Excess Water Content Region 43
D. Approaching The System As A Binary Mixture 46
V. SUMMARY AND CONCLUSION 50
FUTURE WORK 51
REFERENCES 52
APPENDIX 54

LIST OF TABLES

Page

Table I. Portland Cement Types and Characteristics Associated. 5

Table II. The Five Factors Controlling Suspension Rheology, Ranked in Order of Importance. 7

Table III: ASTM Precision of Slump Measurements. 12

Table IV. Concrete Slump Consistency, Range, and Type of Structure. 13

Table V. Material Characterization for Gravel, Sand and Type 1 Portland Cement. 14

Table VI. Gravel and Sand Particle Size Distribution Collected from Standard Sieve Analysis. 15

Table VII. An Example of the Compositions Associated with the Statistical Experimental Matrix along with the Replicants. 18

Table VIII. The Comparison Between the Coarse Tails (5%) with Fine Tails (95%) Particle Size Distribution of Gravel, Sand and Cement. 26

Table IX. The Statistical Experimental Design used to Create the Slump Ternary. 31

Table X. The Slump Ternary Matrix with the Measured Wet Packing Efficiency Values and Standard Deviations Associated with the Compositions. 32

Table XI. The Average Packing Efficiency, Standard Deviation, and Packing Density Associated with Figure 26. 48

LIST OF FIGURES

Page

Figure 1. Specific volume diagram versus weight fraction (Top). An example specific volume diagram versus volume fraction (Bottom).....8

Figure 2. Schematic showing the effect tapping has on the volume of the system along with the addition of water. 10

Figure 3. Schematic showing the four types of slump. 11

Figure 4. Particle size distributions of gravel, sand and cement. 16

Figure 5. Example statistical design ternary diagram comprised of ten compositions. 17

Figure 6. Ternary diagram of the six experimental designs used to determine the optimal dry packing efficiency. 19

Figure 7. Dry packing efficiency versus mixing time used to showing that there was no appreciable change in the packing efficiency over 17 minutes. 21

Figure 8. Photographs of gravel and sand materials. 25

Figure 9. Particle size distributions of gravel, sand and cement with the coarse and fine tails identified as G, S, C is gravel, sand, and cement respectively and subscript C and F are coarse tail (5%) and fine tail (95%).....25

Figure 10. The comparison of dry packing efficiencies predicted versus actual. Superimposed are the experimental design matrices for one and six. 26

Figure 11. All dry packing efficiency data compiled from experimental matrixes one through six presented on one master ternary. 27

Figure 12. (A) The slumping location within the entire ternary plot. (B) The predicted dry packing efficiency data extrapolated from full matrix (Figure 11). (C) The standard error ternary calculated from the

predicted dry packing efficiency data, which was extrapolated from full matrix.....29

Figure 13. Packing efficiency for a 1:1 ratio of sand to gravel with increasing cement content from 0 to 100($^{v}/_{o}$).....30

Figure 14. Experimental matrix that was determined for slump testing. 31

Figure 15. The packing efficiency calculated with the amount of excess water measured within the equivalent stiff slump region. 33

Figure 16. (A) The slumping location within the entire ternary plot. (B) The wet packing efficiency measured within the equivalent stiff slump region. (C) The standard error ternary calculated from the wet packing efficiency ternary diagram. 34

Figure 17. The change in packing efficiency in percent from wet to dry and normalized to the dry packing efficiency of all compositions within the equivalent stiff slump region.....35

Figure 18. (A) The PE_D data extrapolated from full matrix, (B) The PE_W measured within the equivalent stiff slump region, (C) PE_W-PE_D within the slump matrix, (D) The standard error associated with (C). 37

Figure 19. The pore volume displacement compared to the composition of sand within the slump testing matrix (below). The standard error ternary associated with the pore volume displacement. 39

Figure 20. All slump data collected through the experiment separated at ~8 ($^{v}/_{o}$) as a linear region and nonlinear region. 40

Figure 21. The slump values are compared to the excess water using a regression analysis with confidence interval and a prediction band. 42

Figure 22. The pore saturation volume determined based on packing efficiency and the excess water content window calculated for equivalent stiff slump. 43

Figure 23. (A) The slumping location within the entire ternary plot. (B) The excess water that is required at each composition over the equivalent

slump region of 15-45 mm. (C) The standard error ternary calculated from the excess water ternary diagram. 44

Figure 24. A specific volume diagram and excess water content window for composition 70:20:10 (A) and composition 20:20:60 (B). The excess water content window is 3±2 ($^{v}/_{o}$) for equivalent stiff slump. 45

Figure 25. The wet packing efficiency over the area used for slump. The dark lines represent compositions with a constant 10 ($^{v}/_{o}$) and 20 ($^{v}/_{o}$) cement over a range of sand and gravel compositions. 47

Figure 26. This is a two dimensional cross figure of the two dark lines in Figure 25. It represents the predicted wet packing efficiencies over a range of sand and gravel compositions while keeping a constant cement content of 10 ($^{v}/_{o}$) and 20 ($^{v}/_{o}$). 48

Figure 27. Particle size and distribution of gravel, sand and cement. 49

ABSTRACT

Recent work has indicated that the excess water window for typical ceramic forming processes, such as extrusion and tape casting, can be predicted using a specific volume diagram**.** Excess water is defined as the volume of water above that is needed to fill the pore volume. It is proposed that there would be a similar window that correlates with slump behavior for highly loaded systems, such as cements. This thesis identifies a slump window for a typical cement system (gravel, sand, and Portland cement) using a statistical experimental design approach allowing slump behavior to be evaluated over a broad range of compositions and packing efficiencies. The excess water content window for equivalent stiff slump (defined as a slump of 15 to 45 mm) was 3 $^{v}/_{o}$ ($\pm 2^{v}/_{o}$) over the entire composition space. It was also observed that the measured improvement in packing efficiency associated with the addition of water to a dry system was also 3%, exactly the excess volume necessary for equivalent stiff slump. Finally, due to the overlap of the particle size distributions of gravel and sand (aggregate) used in these experiments, it is demonstrated that these cement compositions could be treated as a binary mixture, with the observed optimum in packing efficiency at approximately 80:20 (aggregate:cement) as would be predicted for a binary packing system.

I. INTRODUCTION

Concrete is typically comprised of three raw materials: cement, sand and aggregate. An aggregate is a rock containing of a mixture of minerals. One of the challenges with the production of concrete is that the sand and aggregate used can vary greatly depending on the location. Hydraulic cement is classified as "a material which binds solid bodies together by hardening from a plastic state."[1] In order to understand the composition of the concrete, the raw materials' density, particle size and distribution must be identified. The density, particle size and distribution can vary widely between companies because of the process of crushing or the location where the material is mined. These raw materials are then mixed together with water to be cast for concrete construction.

The majority of the measurements in the concrete industry are performed on a weight basis rather than a volume basis. Since the measurements are performed on a weight basis, a comparison between companies in different regions is difficult due to the change in density and chemical properties of the materials. The densities of the materials used in this experiment were approximately 2.7, 2.8 and 3.2 g/cm^3 of gravel, sand and cement, respectively. On a weight basis, the difference between the three variables is small since the materials are bought in bulk. When measured on a volume basis the difference of 0.47 g/cm^3 will alter the skeletal density of the composition. The current procedure of creating cement suspensions on a weight basis is practical, but must be converted to a volume basis, as the density and volume must be accounted for from system to system.

For typical cements, the densities of sand and gravel range ~2.7 g/cm^3 and the density of cement is ~3.2 g/cm^3. This comes into play because knowing the density allows one to correct for higher densities and other raw materials. This can be applied based on a model, but one still has to measure some packing efficiencies and correct for it. When not corrected for densities, these models do not seem related. This means that the water content associated with a low-density material will be greater than the apparent water content associated with a higher density material. Because the pore volume is the same, the volume of water and powder stays the same but the mass of the powder changes based on the density. The argument is that the change in density does not matter because it will be

corrected for by other factors. When one corrects for the density of the material, everything behaves the same.

The packing efficiency of the aggregate, sand and cement can impact the water level necessary for flow. Changing the packing efficiency of the mixture alters the volume of liquid needed to reach a desired saturation level. A higher packing efficiency reduces the void space, reducing the volume of water required to reach pore saturation. Tap density was used to determine the dry and wet packing efficiency of the mixture. The wet and dry packing efficiencies were compared to determine if the pore volume was altered with the addition of water. As expected, the wet packing efficiency decreased the pore volume and increased the packing efficiency compared to the dry packing.

Particle-particle interactions have an effect on the particle packing of a mixture. The van der Waals attractive forces are an attractive potential that occurs between the particles. When placed in a fluid, the interactions between the molecular dipoles on a particle surface with the surrounding liquid create a small attractive potential which extends out from the particle surface to the liquid. When these forces are combined over an entire particle surface, the net force is no longer insignificant and produces long range particle-particle attractive forces. Although the magnitude of these forces increases with particle size, the attractive potential becomes insignificant when the force of gravity on the particle is greater than the attractive potential between the particles. This is referred to as the colloidal size limit.[2]

Flowability is one of the most important characteristics when working with a cement suspension. A desirable fresh cement mixture must be easy to blend, transport, pour, cast and finish, while; remaining uniform throughout the entire process. The flowability of the concrete structure must be altered depending on the application. This flowability is altered by adjusting the required amount of water within the suspension.

The most popular way of testing the flowability of a cement mixture is the concrete slump test. Concrete slump tests have been established as an ASTM standard C143 "Standard Test Method for Slump of Hydraulic-Cement Concrete."[3] The slump testing procedure has remained unchanged since its introduction in 1922 and is still the primary way to test for the flowability of a mixture. Little research has been done on cement to

produce data that proves a correlation between excess water and flowability on a pore volume basis.

Developing a relationship between excess water and flowability on a pore volume basis for cement mixtures could revolutionize the field. Understanding this relationship could help determine a more precise way to calculate the water required for a specific slump. Recent work on ceramic materials has evaluated the correlation between flowability and the excess water window. In an extrusion process, it was determined that an excess water range between 4-8 volume percent ($^{v}/_{o}$) was required for flow for ground tabular alumina.[4] For tape casting an additional 6-12 ($^{v}/_{o}$)of additional water was ideal for the flow of the suspension.[5] Since a constant window for excess water was discovered for these two processing methods, the idea followed that a similar flow could also be predicted using the slump test. Using a slump test, it was determined that, for optimal slump (between 40-75 mm), excess water content was measured between 0.8-3.8($^{v}/_{o}$) below pore filling using ground tabular alumina.[6] Since this relationship was discovered using ground tabular alumina, a similar relationship was predicted using concrete optimal slump (15-45 mm). It was hypothesized that the excess water content window for uniform slump would be constant regardless of the change in volume percentage of the mixture containing gravel, sand and cement.

II. LITERATURE SURVEY

A. General Background on Portland Cement Concrete

1. Concrete History

The use of concrete as a construction material has been around for thousands of years, dating back to the time of the early Egyptians and Romans. Concrete technology has evolved greatly since that time and is now a billion-dollar industry worldwide and is still growing today. The cement industry in the United States of America produced ~82 million tons of cement in 2015, worth approximately 9.8 billion dollars.[7]

2. Portland Cement

Portland cement was invented in 1824 by Joseph Aspdin "who took out a patent for a cement of superior quality resembling Portland stone, a natural limestone quarried on the peninsula of Portland in England."[8] Portland cement is a hydraulic cement consisting mainly of tri-calcium silicate and di-calcium silicate. When tri-calcium silicate ($3CaO \cdot SiO_2$) and di-calcium silicate ($2CaO \cdot SiO_2$) are mixed with water, it leads to hydrolysis with the bi-products of the reaction being calcium hydroxide ($Ca \cdot (OH)_2$) and a calcium silicate hydrate ($3CaO \cdot 2SiO_2 \cdot 3H_2O$). (Equations 1 and 2).[1] The amount of water required for each of the reactions to occur was calculated by molecular weight and was determined to be 23%, and 21%, respectively, for Equations 1 and 2.

$$2(3CaO \cdot SiO_2) + 6H_2O \rightarrow 3CaO \cdot 2SiO_2 \cdot 3H_2O + 3Ca \cdot (OH)_2 \quad (1)$$

$$2(2CaO \cdot SiO_2) + 4H_2O \rightarrow 3CaO \cdot 2SiO_2 \cdot 3H_2O + Ca \cdot (OH)_2 \quad (2)$$

Due to the wide range of applications of concrete, there are five different types of Portland cement used in industry. The general Portland cement that is most commonly used is "Type 1". Each of the different types of Portland cement vary slightly from each other in order to give them specific properties. Table I below shows the five different types of Portland cement and their general characteristics. There are other types of Portland cement which contain slag, pozzolan material, and other admixtures, however these were not used in this experiment.[8]

Table I. Portland Cement Types and Characteristics Associated.

Type of Cement	General Characteristics
Normal: I	All-purpose cement
Modified: II	Comparative low heat and moderate sulfate resistance
High Early Strength: III	Develops early high-strength and useful when in cold weather
Slow Reacting: IV	Used in mass concrete dams, not common currently
Sulfate Resisting: V	Used in sewers and structure exposed to high sulfates

B. Aggregate

Aggregates are an essential part of the composition of a concrete material, which is comprised of an inert filler material within the Portland cement composition. The aggregate usually occupies 70-75% of concrete by volume; however, this percentage must be controlled to determine the quality of the structure. The three general requirements for the aggregate in industry are the cost of the mixture, the desired strength of the block, and the durability of the structure. Another important characteristic of the aggregate is the gradation of the particle. The gradation of the particle influences the packing density and the arrangement throughout the suspension. To ensure a durable concrete, it is important that the aggregate is resistant to weathering conditions, does not cause any reactions with the cement, and that it contains no impurities that may affect the strength or quality.

Important properties of conventional aggregates are their size distribution, material makeup, morphology, and maximum aggregate size. The two basic morphologies are crushed and round. The crushed morphology aggregates are materials which are crushed at a quarry. Their surfaces are jagged and nonuniform. The round aggregates are typically rounded naturally by water, and require less water than crushed aggregates to achieve the same flowability; however, the crushed aggregates form a stronger bond due to their greater surface area.[9]

The difference between sand and gravel is based primarily on one characteristic, that is, their size. Material that can pass through 3/16 mesh or ASTM sieve size number 4 (4.75 mm) is classified as sand, while larger material is classified as gravel; however, many deposits of sand contain some gravel and vice versa. The sand particles generally consist of an individual mineral of which the most common is quartz. The other minerals remaining are typically feldspars, clays, and impurities like mica and iron. Gravel is heterogeneously comprised of silica, quartz, and granite.[10]

C. Water-to-Cement Ratio

A reduction in the water/-cement ratio relates to a reduction in the shrinkage of a concrete block because there is less water to evaporate. In a cement mixture, a portion of the water is used to determine the flowability of the suspension, while the other part is used for filling the voids between the particles. While an increase in water results in greater flowability, it also reduces structural stability. One of the most widespread tests for the flowability of a cement mixture is the concrete slump test.[11]

The water to cement ratio influences the strength of the concrete. As the water to cement content is decreased, the strength, and durability increase. However, decreasing the water content of the suspension in concrete decreases the workability, which is a critical factor. One solution that is commonly used is the addition of additives which function at low water contents without sacrificing workability.[12] Due to the current interest in high-performance concrete, water content has been closely investigated. Clear comparisons have been made between the decrease in water to cement ratio, and compressive strength. Packing efficiency has also been compared to strength in the past few years. There is an advantage to lowering the water to cement ratio; however there must be enough water added to sufficiently fill up the voids. This amount of water is used to replace the entrained air within the voids. One of the solutions that companies have been employing is the addition of material smaller than Portland cement, such as ultra-fine fly ash which can fill the voids, and thus improve packing density.[13]

D. Specific Volume Diagram

Colloidal suspension rheology is controlled by five factors listed in Table II in order of importance. In plastic bodies, packing of the particles dictates the amount of water within the system. The specific volume diagram is dependent on the packing of particles. Most ceramic forming processes are defined by the amount of water required to enable an operation. The control of the water content classified as a response, is characterized by the three factors: particle-particle interactions, particle size and distribution, and particle morphology. The particle packing of the particles is dictated by three of the following factors: particle-particle interaction, particle size and distribution, and particle morphology. The flowability of a suspension is dictated by the amount of extra room available to the volume provided by the addition of water.

Table II. The Five Factors Controlling Suspension Rheology, Ranked in Order of Importance.[14]

Factor	Description
1	Particle-Particle Interactions
2	Particle Concentration
3	Particle Size and Distribution
4	Particle Morphology
5	Rheology of the Suspension Medium

A specific volume diagram is used to determine the pore volume of the compacted particle and to determine the amount of additional water required for perfect flow.[2] The specific volume diagram yields the pore saturation volume and the density associated with it. The specific gravity of a composition where the pore volume is saturated (υ) as well as the associated weight percent (W_L^*) can be calculated. Figure 1 shows a specific volume diagram versus a weight fraction schematic on top, and on bottom shows a specific volume diagram versus a volume fraction. The diagram on a weight fraction basis creates a problem in accuracy, because even though the mass of the two particles may be equal, the volume which they occupy is different. Creating the specific volume diagram on a volume fraction basis corrects for the density difference and can also be referenced by other

systems. The bottom of Figure 1 shows an example of a specific volume diagram versus a volume fraction for a material with a pore saturation level of 50 (%).

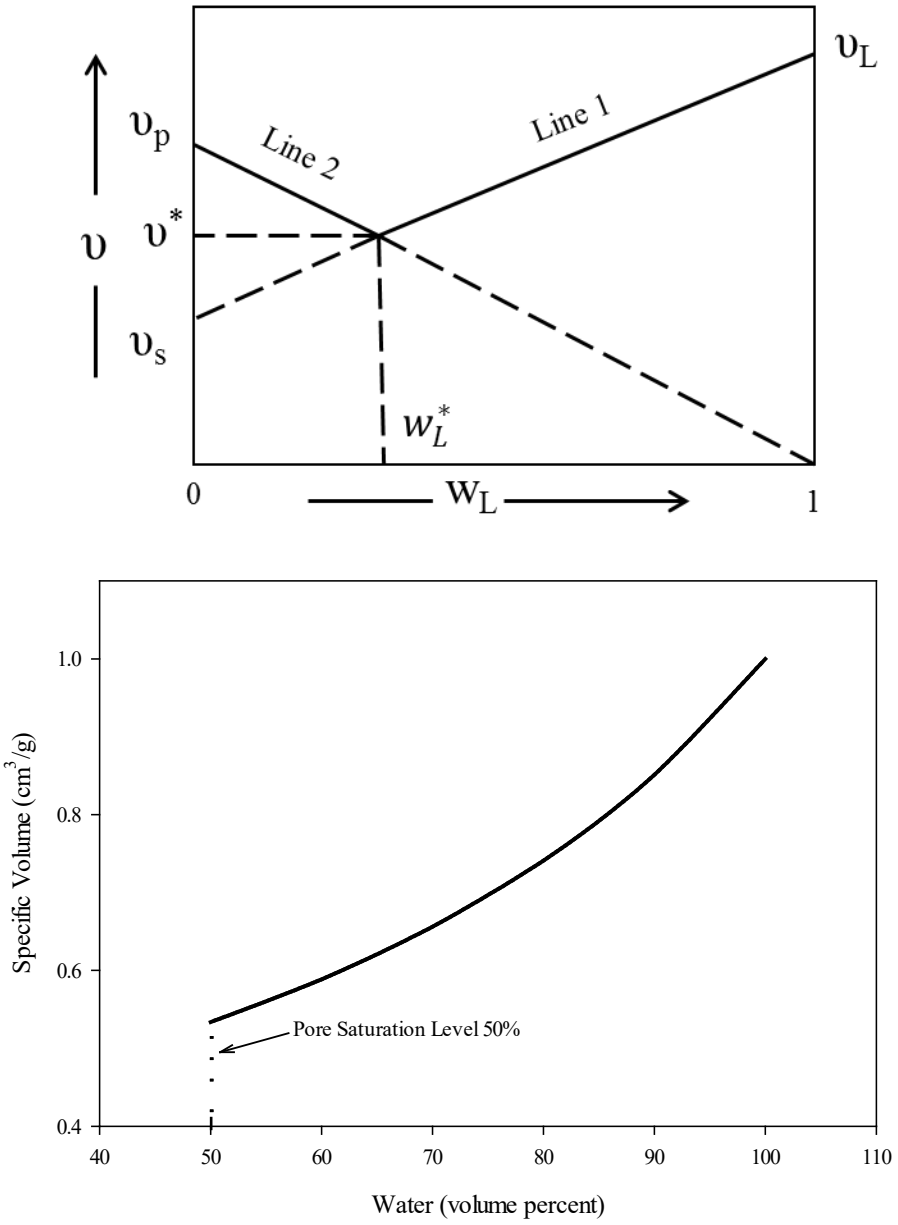

Figure 1. Specific volume diagram versus weight fraction (Top).[15] An example specific volume diagram versus volume fraction (Bottom).

No literature reviews were discovered for deriving a window for slumping via specific volume diagram. This is because in the concrete industry material is typically done on a weight basis rather than volume basis. Other methods such as tape casting and

extrusion have accurately derived windows using a volume approach. The region of excess water percentage was determined using a specific volume diagram on a volume percent basis.

E. Packing Efficiency

In the concrete industry, the packing efficiencies of the coarse and fine materials, the cement, and water content required to fill the pores is critical. However, the proportioning of the mixtures has long been more of an art than a science, and this is clearly indicated by the variety of different methods used worldwide. One of the challenges in the concrete industry is the aggregate, since the aggregates vary in size, shape and chemical makeup depending on their location. Due to the weight of concrete, it is uneconomical to import the material so most aggregates are collected nearby. Particle packing models are founded on the concept that the large particles voids are filled by the smaller particles, thereby reducing the volume of the voids while simultaneously increasing the packing density.[16] The packing efficiency of particles is affected by the number of materials within the mixture. McGeary investigated the particle packing of spherical particles of one, two, three, and four component mixtures and determined the optimum theoretical packing density.[17] Typically for a one component material, the spheres constitute ~60% to 64% of the volume of packing, leaving 40% to 36% voids. For a ternary packing of spheres, the maximum density occurred at of 67 ($^{v}/_{o}$) coarse, 23 ($^{v}/_{o}$) medium and 10 ($^{v}/_{o}$) fine.[17]

F. Water Addition Affecting Packing Efficiency

To determine the excess water required for flowability, it is first important to understand the interaction that water has on the packing efficiency of the mixture. Figure 2 indicates the effect of the tap density approach on the packing of the particle when in a flowable wet mixture. The figure shows the interaction to determine void space by understanding the packing efficiency. The schematic depicts that the addition of water improves the packing efficiency of the suspension. This excess amount of water gives the materials more space to move within the system. The presence of water reduced the Hamaker constant of the material compared to a higher value in air, thereby reducing the attractive potential between the colloidal particles and improving the packing of the

particle-particle interaction.[2] Understanding the cause of the shift in the pore saturation from wet to dry was important, however, determining the extent of the shift was essential for understanding how to create ideal flowability. Flowability testing in the concrete industry is typically done using a slump test.

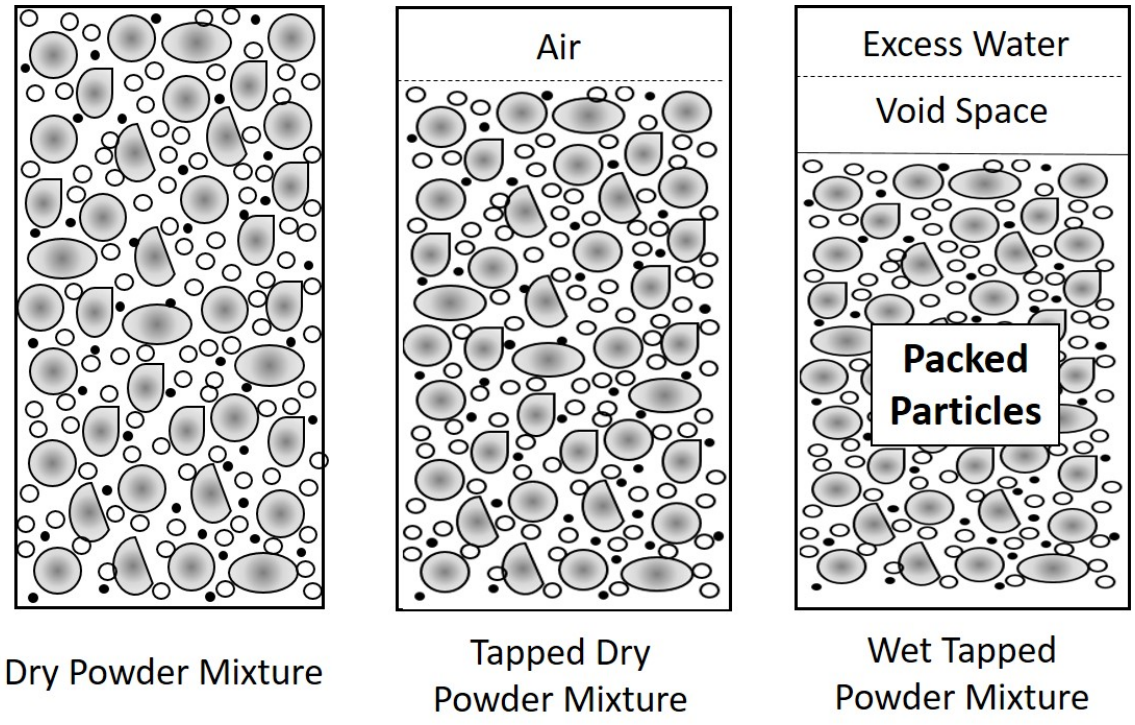

Figure 2. Schematic showing the effect tapping has on the volume of the system along with the addition of water.

G. Slump Testing

Due to its simplicity, the slump testing method has been used extensively all over the world. In the concrete industry, slump testing is used to determine the workability of the suspension. A standard slump test was used.[3] The cement fills the slump cone in three layers using a tamping rod to pack each layer. Slump testing is the most widely used method to evaluate the fluid properties of fresh concrete. It was approved as an ASTM standard in 1922 and has since been used throughout the United States, Europe, and Asia. Advantages to the slump test are that it is relatively inexpensive and small enough to be used at construction sites.[18] This test method is considered applicable to concrete having coarse aggregates up to the size of 1.5 inches (37.5 mm). The typical trend found is that

slumping increases proportionally to the water content within a cement mixture, and slumping is inversely proportional to the strength of the concrete.[3] There are three different types of slump testing: collapse, true slump and planetary mixer type of slump.

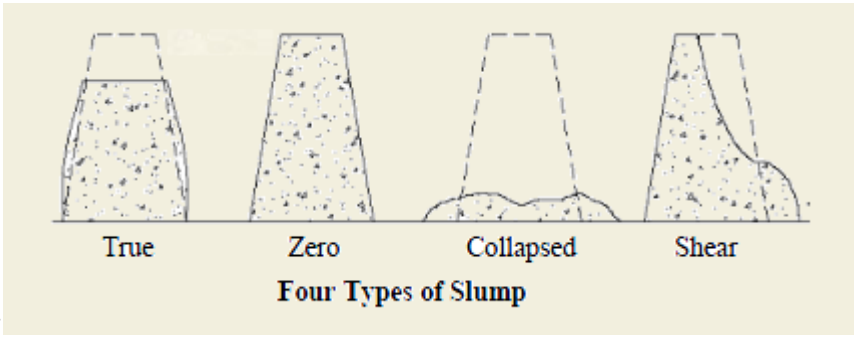

Figure 3. Schematic showing the four types of slump.[19]

Initially there was considerable debate for classifying slump ranges. The ASTM procedure states the acceptable ranges of two results and the precision that each slump test should be rounded to the nearest 5th mm.[3] An example of this would be a 22 mm slump would be 20 mm and the 24 mm slump would be 25 mm rounding to the nearest 5th mm such as 20, 25, 30, 35 mm. The standards were performed by 15 technicians from 14 laboratories using the same truckload of material. The problem is that, in laboratory settings, measurements are typically three or four significant figures and with this material that is not feasible. The ASTM standard recognizes this limitation. One cannot measure to more than 5 mm, which is reasonable since there are aggregates greater than 5 mm. The ASTM acknowledges the size of the aggregate is larger and that is what inhibits the ability to measure. This ± 5 mm is consistent with the aggregate size in this system.

Table III: ASTM Precision of Slump Measurements.[3]

Single-Operator Precision:	**Standard Deviation (1s)**	**Acceptable Range of Two Results (d2s)**
Slump 30mm (1.2 inch)	6 mm (0.23 inch)	17 mm (0.65 inch)
Slump 85 mm (3.4 inch)	9 mm (0.38 inch)	25 mm (1.07 inch)
Slump 160 mm (6.5 inch)	10 mm (0.40 inch)	28 mm (1.13 inch)

Within the ASTM standard, however there is no standard for the ranges at which to classify the slumps since it is chosen on an industrial basis. This reason relates to the aggregates and the Portland cement used because most of the materials are acquired near the site where the cement is used. Due to this, the composition of the mixture and size and shape of the coarse, medium, and fine, makes defining a uniform slump range difficult. Another challenge has been that the range for slump is dependent on the project, since each consistency relates to a different structure. One source that has published an arbitrary range of slumps and varying degree of consistencies which can be used as a reference as presented in Table IV following the ASTM standard. The temperature can also affect the consistency of the mixture, however, since these tests are meant to be applied on site this is an uncontrollable variable.[9]

Table IV. Concrete Slump Consistency, Range, and Type of Structure.

Consistency	Slump	Type of Construction
Dry	0-1 in 0-25 mm	Not applicable
Stiff	0.5-2.5 in 10-65 mm	Massive, Semi-massive
Medium	2-5.5 in 50-140 mm	Heavy Building
Wet	5-8 in 130-200 mm	Heavy Building, Light
Sloppy	7-10 in 180-255 mm	Not applicable

- **Massive**: Dams, Heavy piers, large open foundations.
- **Semi-Massive**: Piers, Heavy Walls, Foundations, Heavy arches.
- **Heavy Building**: Small Piers, medium footings, wide spacing of reinforcement.
- **Light**: Small structural members, thin slabs, small columns, closely spaced reinforcement.

III. EXPERIMENTAL PROCEDURE

A. Raw Materials

A commercial cement was used (Type 1 Saylors iWork Portland Cement, Essroc Cement Corp, Nazareth, PA). Gravel and masonry sand was obtained locally (Southern Tier Concrete, Alfred, NY). All the material was dried 110°C before use. The specific surface area was determined using a multiple point BET method (Tristar II BET, Micromeritics, Norcross, GA) and the density of the materials were determined using a helium pycnometer (Accupyc II 1340, Micromeritics, Norcross GA). These values are presented in Table V.

Table V. Material Characterization for Gravel, Sand and Type 1 Portland Cement.

Material	**Gravel**	**Sand**	**Cement**
Density (g/cm^3)	2.68	2.76	3.15
Specific Surface Area (m^2/g)	N/A	N/A	0.02

B. Particle Size

Sieve analysis on gravel and sand was conducted using a standard method[20] and were compiled in Table VI. The D_{50} of the gravel and sand were 4.75 mm and 1.0 mm respectively. For Portland cement, a laser scatter technique was used (LS13320 Multiwavelength, Beckman Coulter, Indianapolis, Indiana). The Portland cement powder was placed in water and ultrasonicated for two minutes with no dispersant. The particle size distributions of gravel, sand and cement are presented in Figure 4.

Table VI. Gravel and Sand Particle Size Distribution Collected from Standard Sieve Analysis.

Sieve Opening (mm)	**Sieve Number**	**Cumulative Mass Finer Than Gravel (%)**	**Cumulative Mass Finer Than Sand (%)**
8	5/16	99.16	-
6.3	1/4	81.60	-
4.75	4	48.69	99.12
3.35	6	18.39	92.69
2.36	8	6.56	80.71
2	10	3.18	
1.7	12	2.64	68.58
1.4	14	2.29	62.78
1.18	16	2.09	57.25
1	18	-	51.90
0.85	20	1.80	46.78
0.71	25	-	41.91
0.6	30	-	36.66
0.425	40	-	28.14
0.354	45	-	23.61
0.3	50	-	19.35
0.25	60	-	15.56
0.212	70	-	11.38
0.15	100	-	6.78
pan	>100	-	-

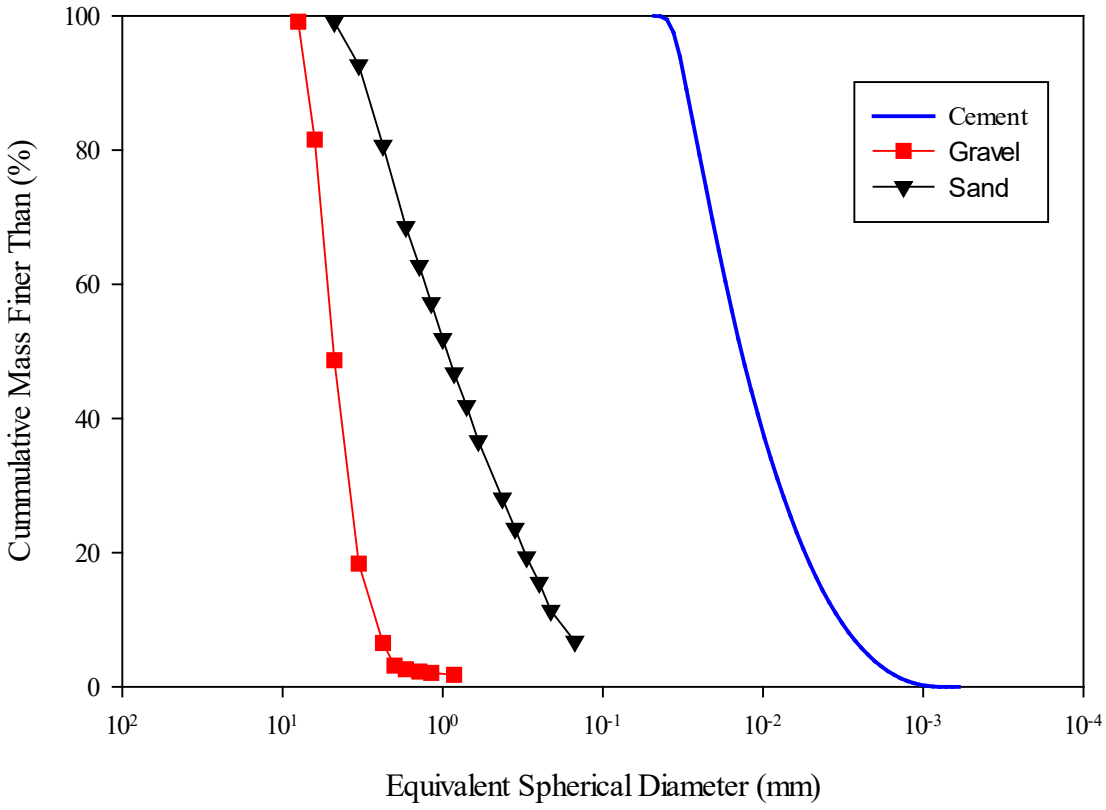

Figure 4. Particle size distributions of gravel, sand and cement.

C. Design of the Experiment

Commercial statistical experimental design software, (Design-Expert, v.9, Stat-Ease, New Lexington, Ohio) was used to develop the statistical experimental designs. Batching was done on a volume basis, and all experiments were conducted in random order. The values initially ranged from 0-100 (%) and then the ranges were narrowed. The ten compositions of an example ternary diagram are listed in Table VII and plotted in Figure 5. The replicants were the three corners of the ternary diagram and then another point selected randomly. Six experimental designs (Figure 6) were constructed. The first statistical experimental design centered on the predicted ratio for optimum packing: 70:20:10 ratio of gravel, sand and cement, respectively. This ratio (70:20:10) did not produce the maximum packing efficiency because the particle size distributions of the three materials (gravel, sand and cement) failed to meet the recommended 100:10:1 ratio.[17] The

14 data points for each of the six statistical designs in Figure 6 are presented in Appendix A.

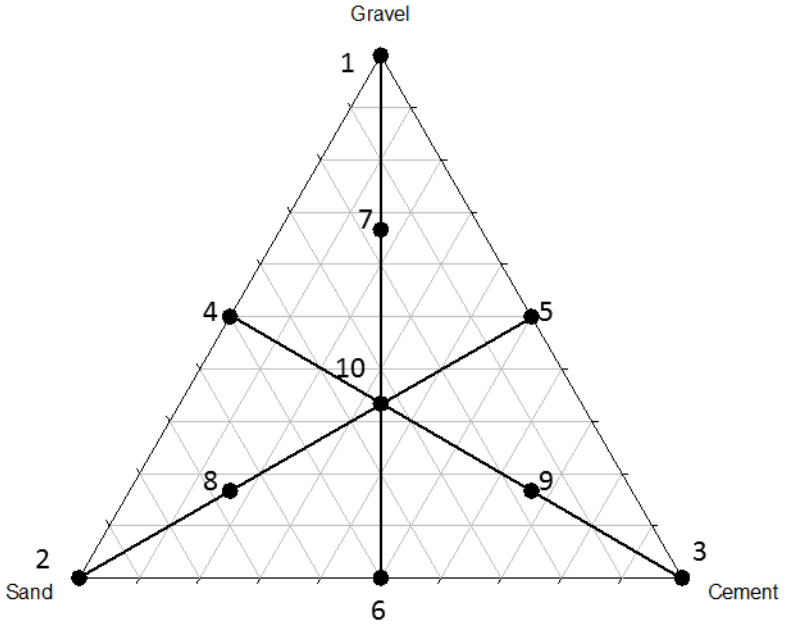

Figure 5. Example statistical design ternary diagram comprised of ten compositions.

Table VII. An Example of the Compositions Associated with the Statistical Experimental Matrix along with the Replicants.

Standard Order	Replicants	Gravel	Sand	Cement
1	11	100	0	0
2	12	0	100	0
3	13	0	0	100
4	-	50	50	0
5	-	50	0	50
6	14	0	50	50
7	-	66.6	33.3	33.3
8	-	33.3	66.6	33.3
9	-	33.3	33.3	66.6
10	-	33.3	33.3	33.3

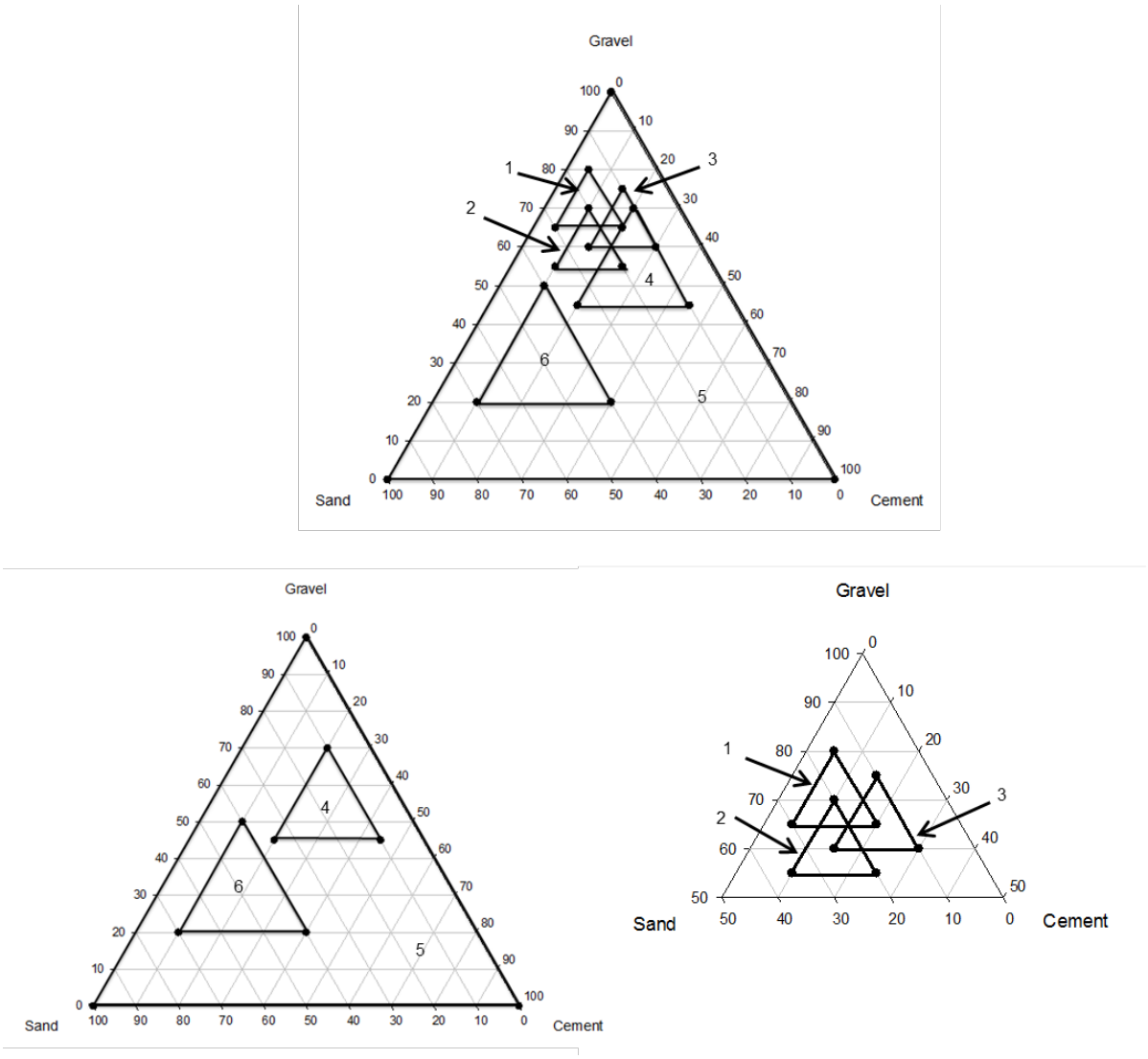

Figure 6. Ternary diagram of the six experimental designs used to determine the optimal dry packing efficiency.

D. Packing Density Measurement

1. Dry Packing Density

The dry packing efficiency was determined using a tap density approach (Dual Autotap, Model DAT-6, Quantachrome Instruments, Boynton Beach, Florida). The compositions were placed into a plastic container and ball milled for 30 minutes. A polypropylene 500 ml graduated cylinder was used for dry packing efficiency, and 1000 ml graduated cylinder was used for wet packing efficiency measurements. The graduated cylinder was calibrated using water. The two cylinders gave similar packing efficiency results, when the same composition was tapped in both the 1,000 ml and 500 ml graduated cylinder. A total of 10,000 taps were performed for each experiment consistent with work previously done.[4] The dual autotap machine had a tapping rate of 4 minutes per 1,000 taps (~4 cycles per second).

2. Rule of Mixtures (R.O.M.)

The rule of mixtures can be used to calculate the density of a mixture

$$f_{(A,V)} \cdot \rho_{(A)} + f_{(B,V)} \cdot \rho_{(B)} + f_{(C,V)} \cdot \rho_{(C)} + \cdots f_{(n,V)} \cdot \rho_{(n)} = \rho_{(sample)} \quad (3)$$

Where, $f_{(A,V)}$ is the volume fraction of component A, $\rho_{(A)}$ is the density, and $\rho_{(sample)}$ is the density of the composite sample. The sum of the fractions equal 1.0:

$$f_{(V,P)} + f_{(V,W)} + f_{(V,A)} = 1.0 \quad (4)$$

Where, $f_{(V,P)}$ is the volume fraction of powder. $f_{(V,W)}$ is the volume fraction of water: and $f_{(V,A)}$ is the volume fraction of air. To determine density using a mass basis, $f_{(X,m)}$ the specific volume (v) must be used:

$$v_A = \frac{1}{\rho_A} \quad (5)$$

$$f_{(A,m)} \cdot \left(\frac{1}{\rho_A}\right) + f_{(B,m)} \cdot \left(\frac{1}{\rho_B}\right) + f_{(C,m)} \cdot \left(\frac{1}{\rho_C}\right) + \cdots + f_{(n,m)} \cdot \left(\frac{1}{\rho_n}\right) = \left(\frac{1}{\rho_{sample}}\right) \quad (6)$$

3. Mixing Time

A planetary mixer (Hobart, Model D-300, Troy, Ohio) was used to mix both wet and dry material. To determine a mixing time (as shown in Figure 7) samples were extracted over a period of 17 minutes at three minute intervals starting at two minutes mixing. The density measured no appreciable change in packing efficiency over that time

interval, so five minutes was selected. Since there were no significant differences in the packing efficiencies over the 17 minutes it was assumed that the material was mixed uniformly.

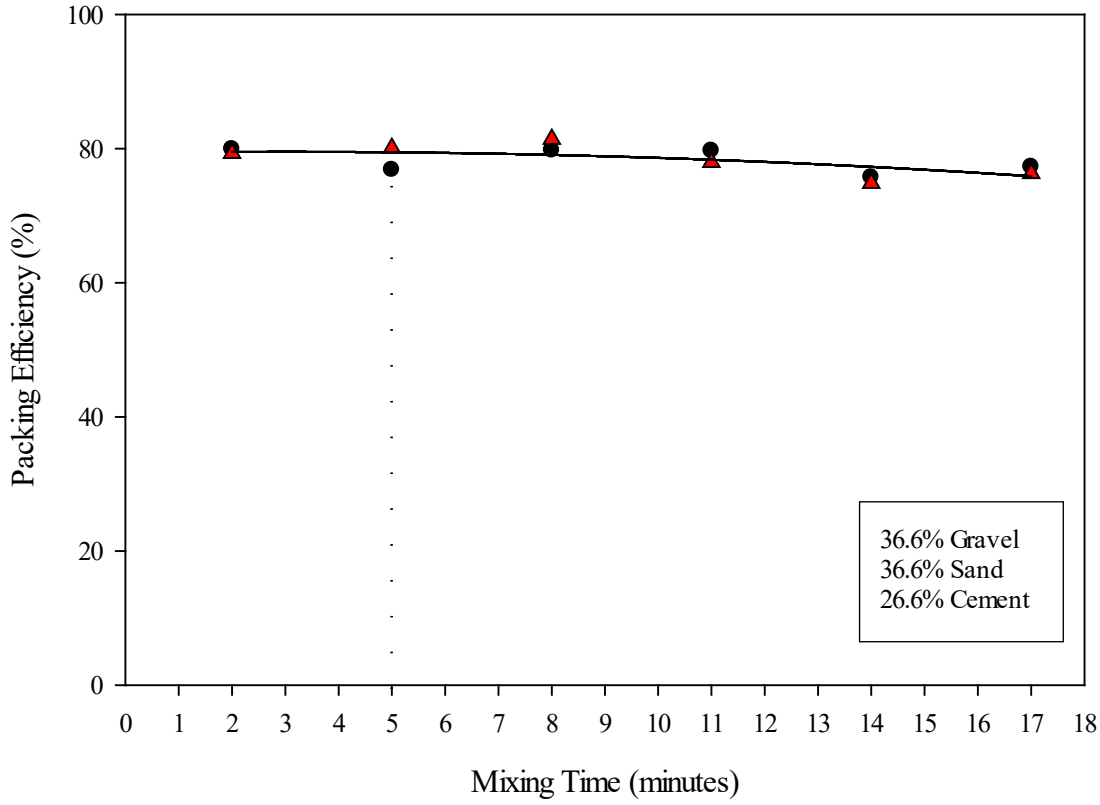

Figure 7. Dry packing efficiency versus mixing time used to showing that there was no appreciable change in the packing efficiency over 17 minutes.

4. **Wet Packing Density**

The wet tap density procedure used extracted specimens from slump test samples. It is not common to perform tap density on a wet material. The decrease in volume overall was evident by the gas bubbles in the system being released. A process for wet packing density was developed. The procedure consisted of collecting the sample by scooping the material out of the top of the mixer. This was done under the assumption that there was no segregation by particle size. The ASTM standard for slump uses a tamping rod to compact the wet mix and release entrained air within the slump cone at three stages. Two 1000 ml

graduated cylinders were filled for tap density measurements; the slump testing was performed during the tapping cycle.

To determine the volume of the packed particles, the packed bed height was measured with a rod inserted into the graduated cylinder. After the excess water in the system was measured, the volume was subtracted from the overall tapped volume to determine the volume of powder. A rule of mixtures approach was used to calculate the volume of water and powder within the graduated cylinder. After the mass and volume of the material in the graduated cylinder was measured, the material was placed back into the planetary mixer and 2 ($^{v}/_{o}$) water was added based on the total 7200 cm^3 volume. Then the material was mixed for five minutes and the procedure was repeated three more times increasing the water amount with each water addition (based on the initial sample volume). The amount of water within the sample was based on the amount that was present within the graduated cylinder, which was calculated by the packing efficiency of the powder within the water and the excess water present.

E. Slump Testing

1. Determining Water Content for Slump Test Calculations

Each of the packing efficencies for the slump testing were extrapolated from the dry packing efficiency data. Equation 7 was used to calculate the pore volume (V_P) :

$$V_P = V_B * (1 - PE) \quad (7)$$

Where V_B is the total volume of the batch, and PE is the packing efficiency.

2. Slump Test Procedure

The compositions of the slump tests were determined based on the calculated dry packing efficiency data. The slump test followed the standard procedure.[3] 7200 cm^3 of material was enough material to use for slump testing along with two tap density tests with 1000 ml graduated cylinders. All samples for slump were mixed in a Hobart mixer for five minutes before the addition of water. The initial amount of water added into the mixture varied depending on the composition and the dry packing efficiencies. Water was then introduced into the mixer in ≤30 seconds while mixing and then mixed for an additional

five minutes. The material was first taken out of the planetary mixture and placed into the graduated cylinders to measure wet tap density. The remaining material was used to complete the slump test (measured in millimeters) which was done using a standard steel slump cone (Steel Slump Cone, Model HM-45M, Global Gilson, Lewis Center, Ohio) on top of a steel plate. After the slump testing was completed, the material was returned to the planetary mixer and the cycle repeated after increasing the water volume. Volumes were not corrected for any losses that occurred through transfer. The slump testing typically was completed in approximately 1 hour so that any concern of the cement setting was disregarded.

IV. RESULTS AND DISCUSSION

A. Determining Packing Efficiency Using Tap Density

1. Dry Packing Density

The void space within a mixture is dictated by the packing efficiency. Figure 8 shows the photographs of gravel and sand**.** There is significant overlap in the particle size and distribution of sand and gravel as shown in Figure 9. Both of the gravel and sand measurements were determined using the sieve analysis method, while cement used a laser scattering technique. The particle size of sand overlapped 49 percent of the gravel particle size and distribution. This overlap in the gravel and sand affects the particle packing of the composition because neither material is large or small enough to fit in-between one another. The particle size ratios do not fit what is predicted to be necessary in the literature of 100:10:1 of coarse:medium:fine.[17] The coarse tail (95%) and the fine tail (5%) of the particle size and distribution lines are compiled in Table VIII. These values were then used to determine the ratio size in Table VIII. The ratio of gravel to sand was 1:1.85 (i.e., the fine tail of the gravel is smaller than the coarse tail of the sand) clearly failing to meet the necessary 10:1 size ratio.[17] The. The sand:cement ratio also failed to meet the 10:1 size ratio with the cement with a ratio of 3.5:1. The gravel:cement ratio, however, exceeded the 10:1 size ratio with a ratio of 57:1. The sand particle and size distribution failed to meet the predicted size ratio for maximum packing efficiency of a ternary mixture for both the coarse and fine. If particle size and distribution were consistent with the 100:10:1 ratio, the ratio of materials expected would have been 70:20:10. Since the sand did not meet the particle size and distribution ratio, the maximum packing efficiency was 25:60:15 of gravel, sand and cement respectively. Figure 10 illustrates this difference between the predicted and measured compositions necessary to achieve maximum packing efficiency.

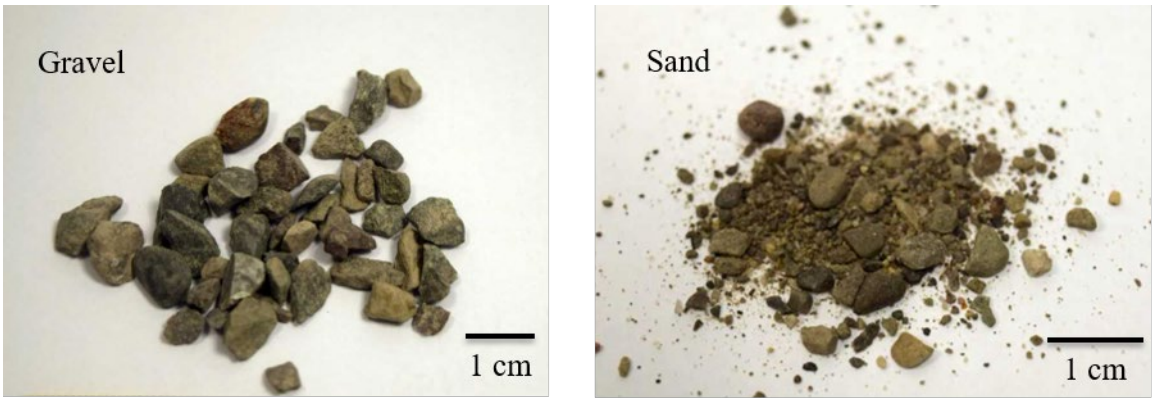

Figure 8. Photographs of gravel and sand materials.

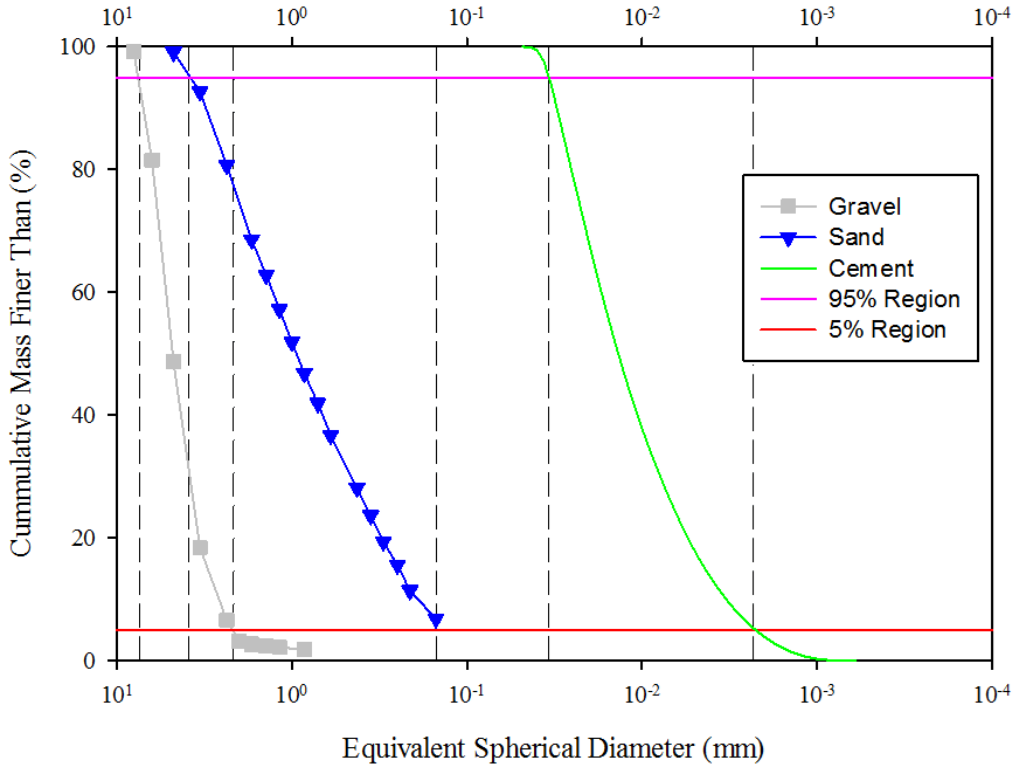

Figure 9. Particle size distributions of gravel, sand and cement with the coarse and fine tails identified as G, S, C is gravel, sand, and cement respectively and subscript C and F are coarse tail (5%) and fine tail (95%). The figure displays that there is significant overlap within the gravel and sand, while the only material to satisfy the 10:1 ratio of coarse to fine is the gravel:cement ratio.

Table VIII. The Comparison Between the Coarse Tails (5%) with Fine Tails (95%) Particle Size Distribution of Gravel, Sand and Cement. This Comparison was used to Determine Whether the 10:1 Particle Size Ratio was Satisfied.

Material	Large (5% CMFT)	Small (95% CMFT)	Ratio	Meet Ratio Target 10:1
Gravel:Sand	2.1 mm	3.9 mm	1:1.85	No
Gravel:Cement	2.1 mm	37 μm	57:1	Yes
Sand:Cement	0.13 mm	37 μm	3.5:1	No

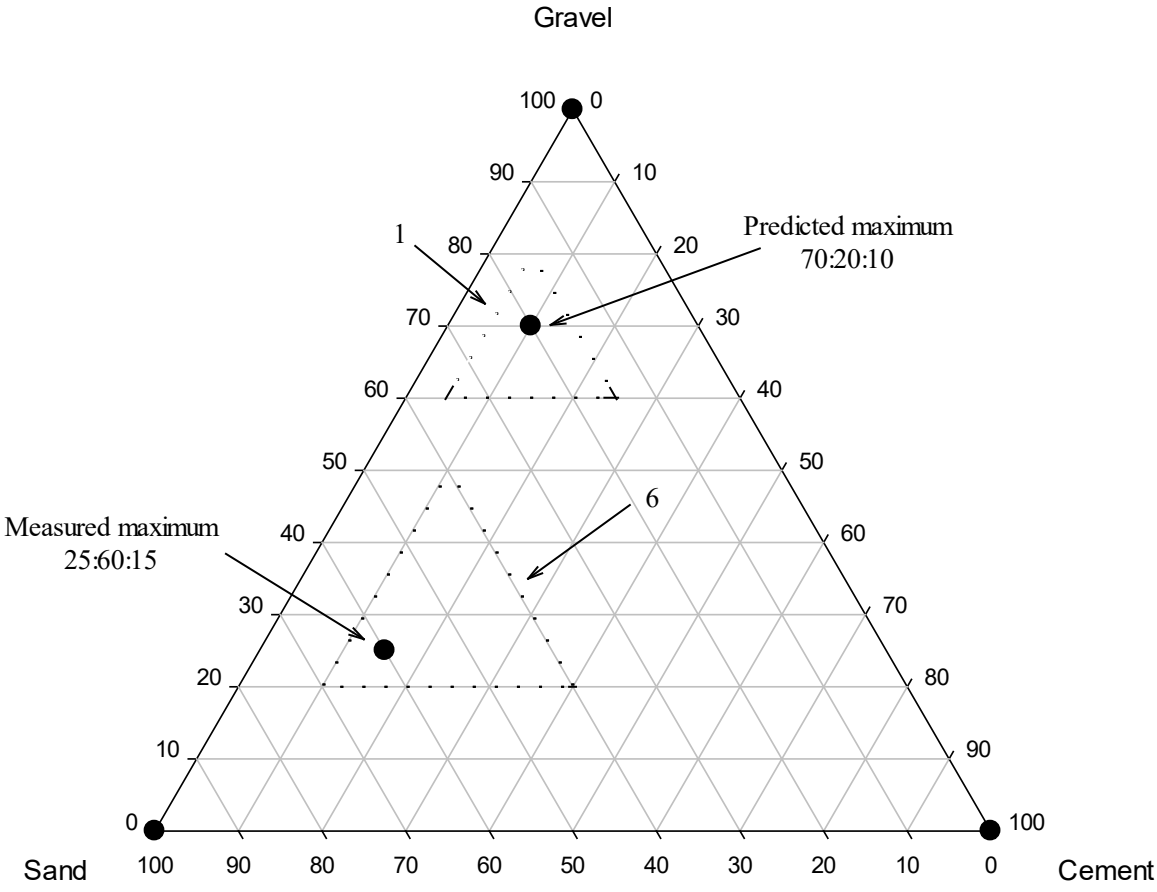

Figure 10. The comparison of dry packing efficiencies predicted versus actual. Superimposed are the experimental design matrices for one and six.

All the data was compiled into a master plot (figure 11). The packing efficiency values and compositions used to calculate the master ternary plot are in Appendix A. The packing efficiency of the gravel, sand and cement individually were 56%, 65%, and 42%, respectively. Packing efficiency contour lines are listed at 50, 60, and 70 and in the middle of the oval region is the optimum packing efficiency. The dots represent the data from all of the dry statistical experiments combined and the numbers next to the dots represent number of replicants. So as is evident in the figure there was a higher concentration of data in higher gravel levels because that was previously predicted to be the optimum packing efficiency. Then the matrix was expanded eventually finding the optimum far away from what was predicted as was illustrated in Figure 10. When blended, the three materials produced a maximum packing efficiency of 76%. The results in Figure 11 indicate that the composition 25:60:15 (gravel:sand:cement) achieved the highest dry packing efficiency.

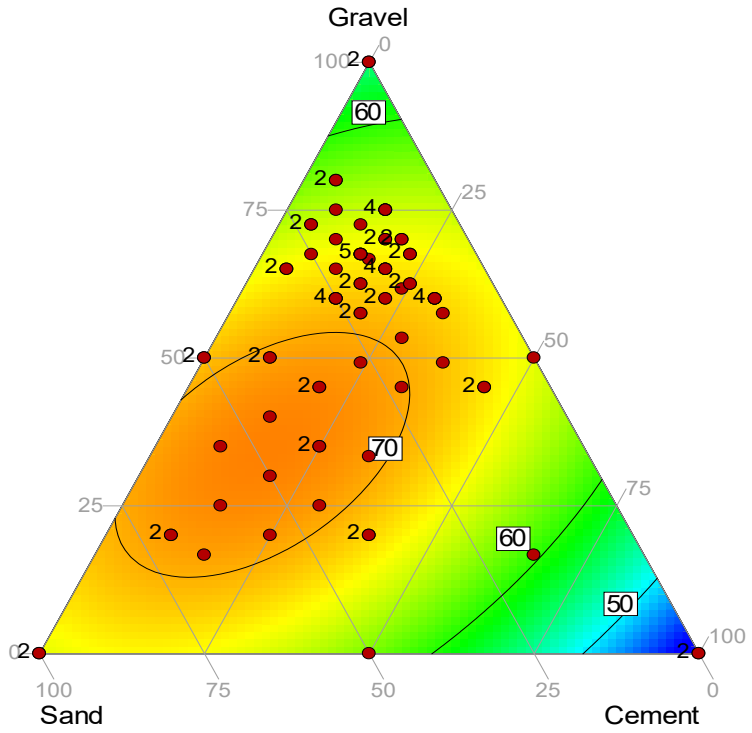

Figure 11. All dry packing efficiency data compiled from experimental matrixes one through six presented on one master ternary. Dry packing efficiency regions are identified using the contour lines.

Figure 12 is the experimental matrix for slump testing extrapolated from the entire dataset shown in Figure 11. The predicted moisture sensitivity of cement[12] was not

observed. The slump test matrix was designed to evaluate the cement contribution at different aggregate levels while keeping the gravel to sand ratio constant. The dotted line in Figure 14 shows an increasing cement level, while the ratios of sand to gravel remain constant. As the cement level in the mixture decreased from 60 ($^{v}/_{o}$) to 10 ($^{v}/_{o}$), the packing efficiency increased from 59% to 72%, shown in Figure 12. Figure 13 combines the data from Figure 11 and 12 to display how the cement content influenced the packing efficiency while the sand and gravel ratio remained constant. The maximum packing efficiency is obtained by a cement content between 10 ($^{v}/_{o}$) and 20 ($^{v}/_{o}$)which links to a binary system approach of 80:20 ratio of coarse to fine particles (discussed later).

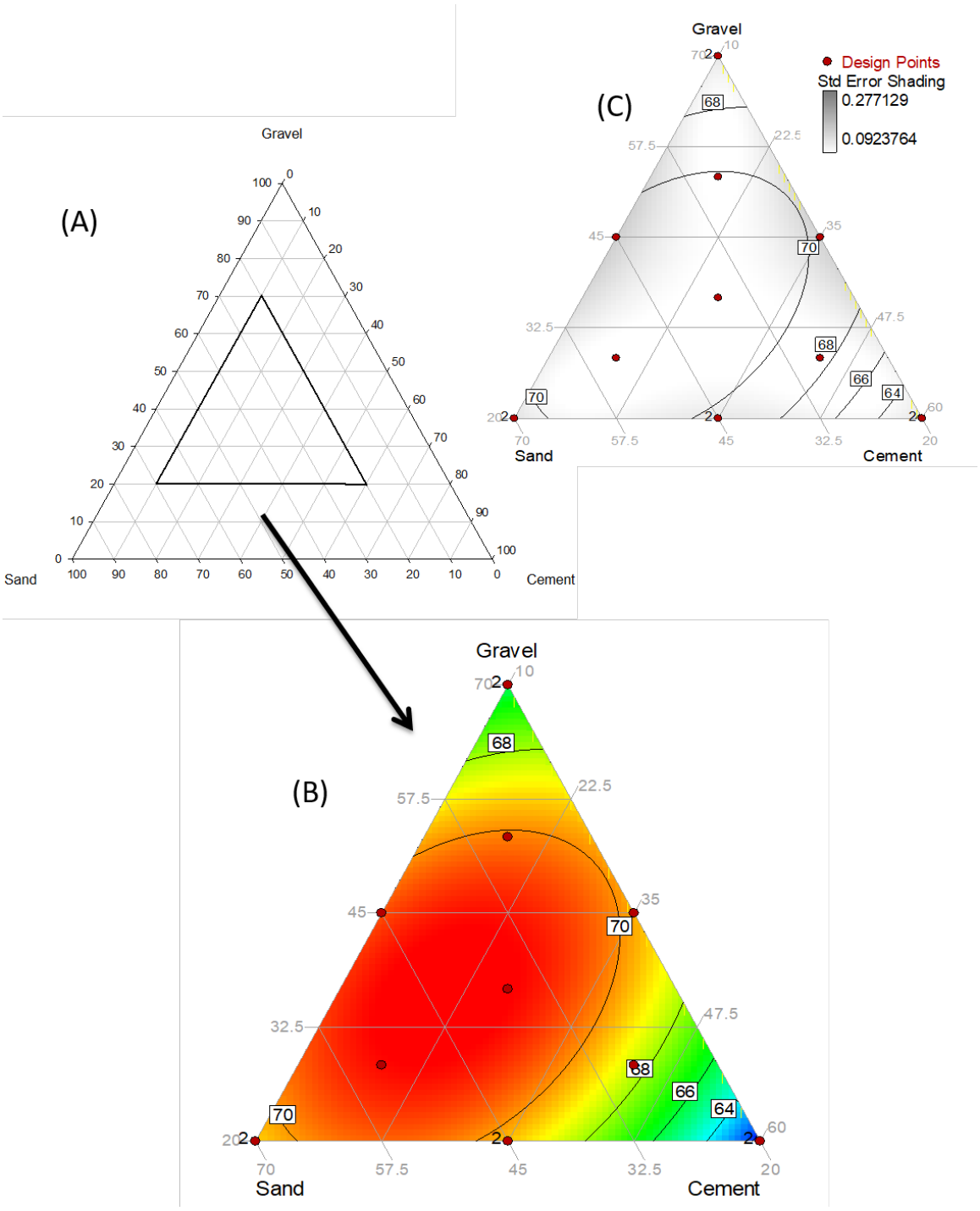

Figure 12. (A) The slumping location within the entire ternary plot. (B) The predicted dry packing efficiency data extrapolated from full matrix (Figure 11). (C) The standard error ternary calculated from the predicted dry packing efficiency data, which was extrapolated from full matrix.

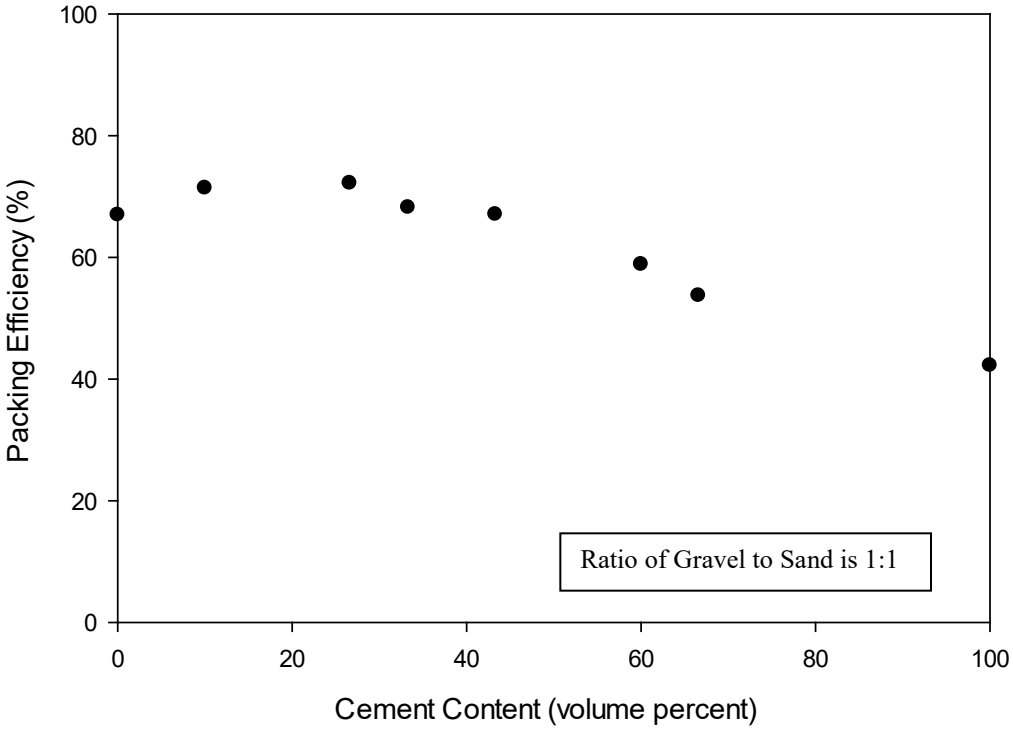

Figure 13. Packing efficiency for a 1:1 ratio of sand to gravel with increasing cement content from 0 to 100($^{v}/_{o}$). Showing that the optimum packing efficiency occurs between the 10 ($^{v}/_{o}$) and 20 ($^{v}/_{o}$) cement region.

2. **Slump Test Procedure**

A stiff consistency slump range of 30±17 mm was selected. Since the standard requires the nearest 5th mm, for the purpose of this analysis 30±15 mm was defined as an "equivalent stiff slump." Accordingly, a slump of 45 mm is considered equivalent to a slump of 15 mm. The slump test matrix is represented in Figure 14 with the compositions in Table IX.

Table IX. The Statistical Experimental Design used to Create the Slump Ternary. Attached are the Predicted Dry Packing Efficiency Values Associated with the Compositions.

Standard Order	Run Order	Gravel	Sand	Cement	Dry Packing Efficiency
1	1,8	70	20	10	66
2	4,11	20	70	10	73
3	6,7	20	20	60	59
4	5,14	20	45	35	70
5	13	53.3	28.3	18.3	71
6	9	28.3	53.3	18.3	73
7	3	28.3	28.3	43.3	67
8	10	45	20	35	69
9	12	45	45	10	71
10	2	36.6	36.6	26.6	72

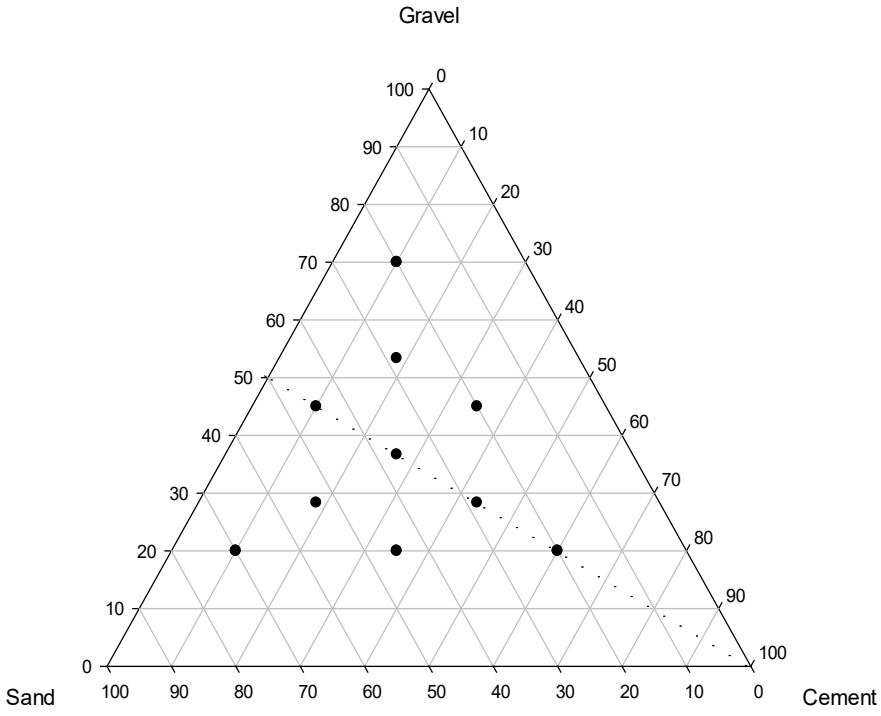

Figure 14. Experimental matrix that was determined for slump testing. The dotted line represents the increase in cement content, while keeping the sand to gravel ratio constant at 1:1.

3. **Wet Packing Density**

The packing efficiency in the previous section was used to determine the amount of water required to fill the pore volume. The volume percentages of gravel, sand and cement of the 14 compositions are listed in Table X. The replicants range from two to twelve measurements. The standard deviation of the wet packing efficiency ranged from 5% to 1% (Table X). The packing efficiency increased slightly with the addition of water shown in Figure 15. Once water is added, the packing efficiency, however, is independent of excess water.

Table X. The Slump Ternary Matrix with the Measured Wet Packing Efficiency Values and Standard Deviations Associated with the Compositions.

Standard Order	Run Order	Gravel	Sand	Cement	Average Wet Packing Efficiency	Standard Deviation
1	1,8	70	20	10	73	5
2	4,11	20	70	10	74	1
3	6,7	20	20	60	63	3
4	5,14	20	45	35	71	3
5	13	53.3	28.3	18.3	73	1
6	9	28.3	53.3	18.3	76	1
7	3	28.3	28.3	43.3	66	4
8	10	45	20	35	67	3
9	12	45	45	10	75	2
10	2	36.6	36.6	26.6	75	1

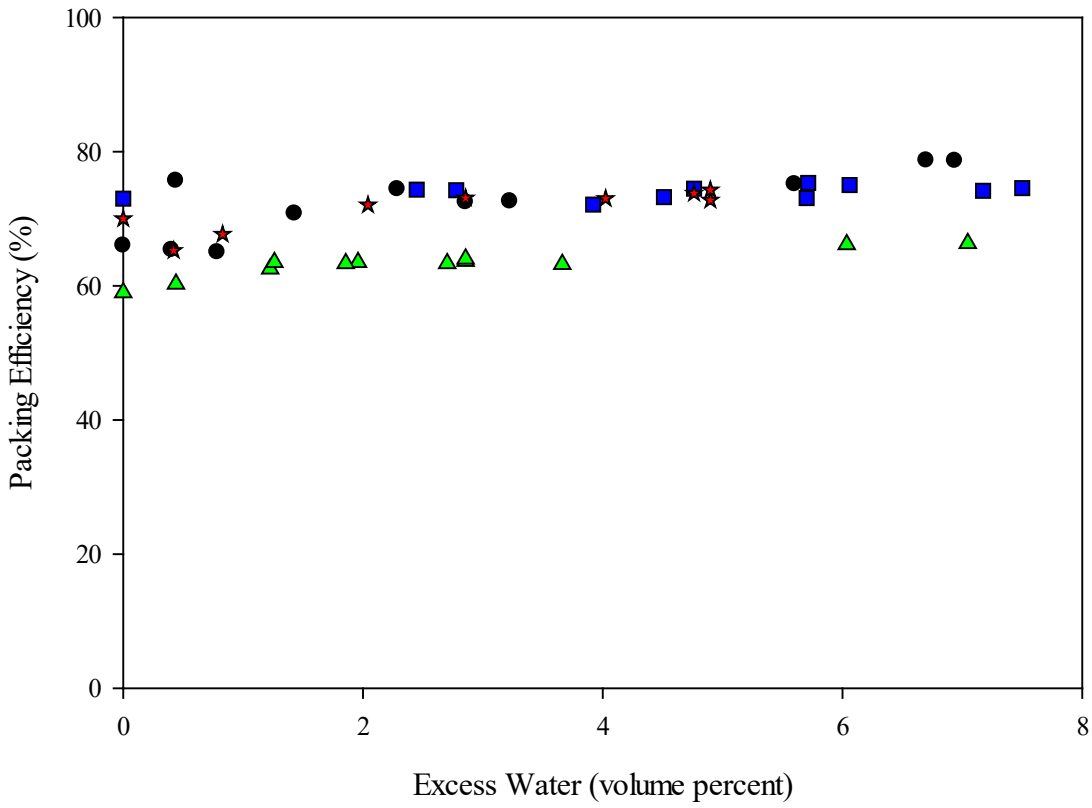

Figure 15. The packing efficiency calculated with the amount of excess water measured within the equivalent stiff slump region. Compositions displayed are standard order 1 (●), 2(■), 3(▲), 4(★) comprised of 70:20:10, 20:70:10, 20:20:60, and 20:45:35 volume percentage of gravel, sand and cement, respectively.

Certain compositions had more replicants than others and varied at different excess water content regions. The replicants are displayed in the ternary diagrams with the number next to the data points. The wet packing efficiencies in Table X were used to create Figure 16. Figure 16 used all of the wet packing efficiency values for each of the compositions that were within the equivalent stiff slump region. The ternary diagram shows that as the cement content within the structure decreases the packing efficiency increases. Ranging from 63% (high cement) to 75% (low cement). The standard error ($\frac{Standard\ Deviation}{\sqrt{Sample\ Size}}$) is minimal throughout the experimental matrix.

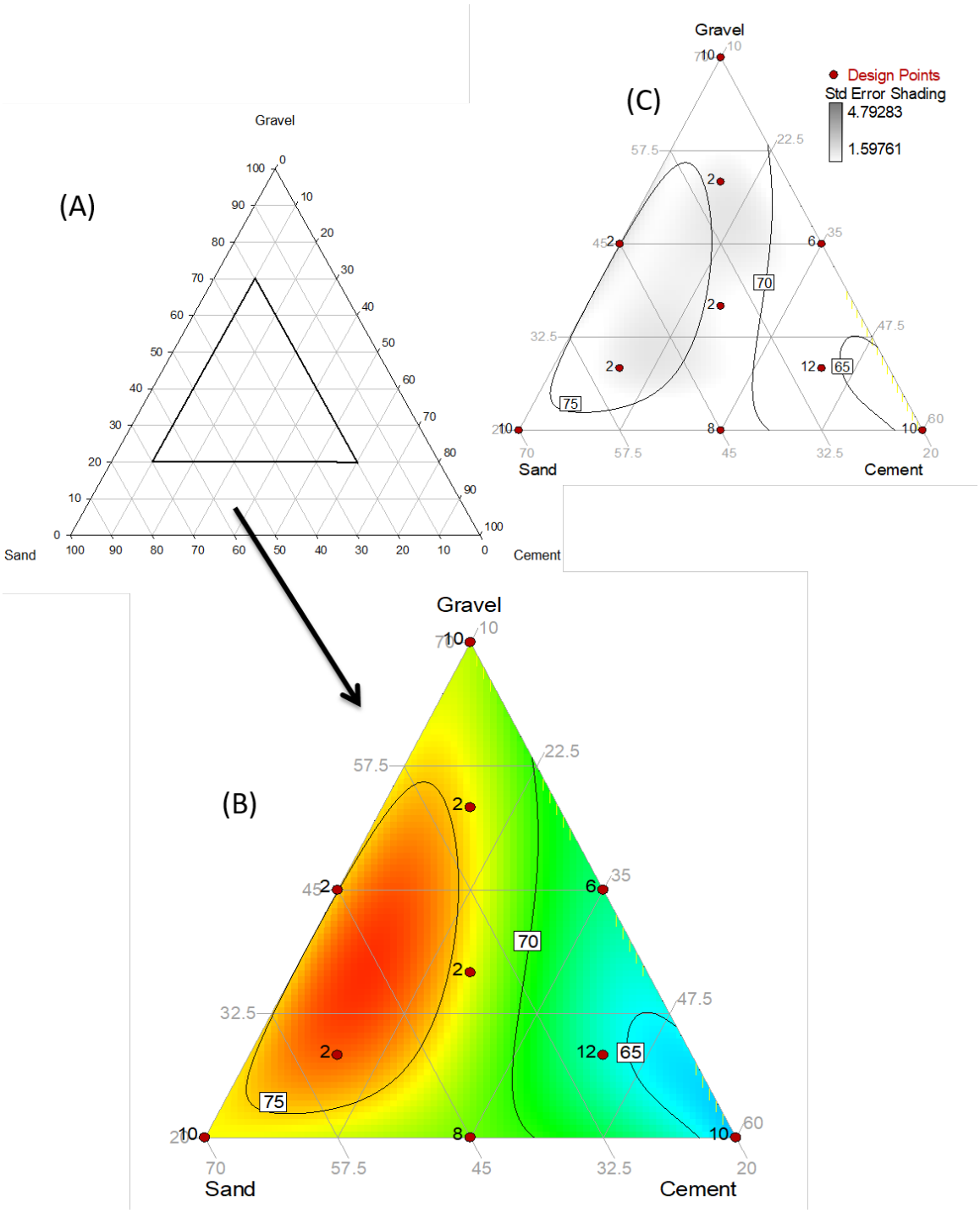

Figure 16. (A) The slumping location within the entire ternary plot. (B) The wet packing efficiency measured within the equivalent stiff slump region. (C) The standard error ternary calculated from the wet packing efficiency ternary diagram.

The change in packing efficiency was calculated on a percentage basis (Equation 8); normalized to the dry packing efficiency.

$$\frac{(PE_{wet}-PE_{dry})}{PE_{dry}} = Change\ in\ Packing\ Efficiency(\%) \quad (8)$$

The overall improvement from dry to wet packing efficiency on a percent basis, was 3%±6.4%. This decreases the amount of water necessary to fill the pores and the entrainment of air contributes to the error in the slump. The water content necessary to create a slump of 15-45 mm is presented in Figure 17. The wet packing efficiency was normalized to the dry packing efficiency for each composition and showed that the addition of water improved the overall packing efficiency percent by 3±6.4%. The trend in the plot indicates that there is a small increase in packing density with increasing excess water, but regression analysis generates an r^2 value of 0.2 indicating this is a weak trend at best, accounting for only 20% of the data.

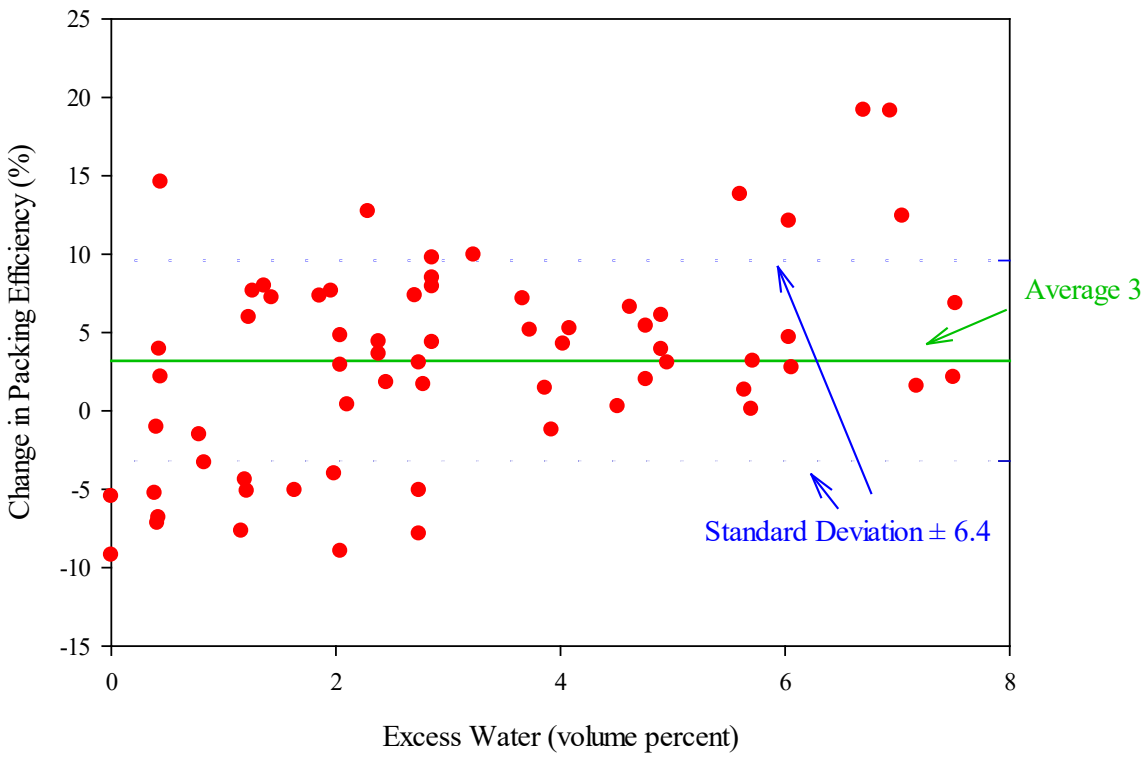

Figure 17. The change in packing efficiency in percent from wet to dry and normalized to the dry packing efficiency of all compositions within the equivalent stiff slump region.

Figure 18 compares wet (PE_W) and dry (PE_D) packing efficiencies. Figure 18 presents the packing efficiency difference as an absolute value related to the initial (dry) packing behavior rather than as a percentage (normalized to the dry packing efficiency value). The packing efficiency values range from 7% to -2%. The standard error ternary diagram, show that none of the predicted values varied by more than 0.5 times the standard deviation of the mean.

In this study, there is a correlation between the dry packing efficiency and the ideal amount of excess water necessary for slump based on the improvement of packing density of the powder with the addition of the water. The improvement of packing density was 3 ±2 ($^{v}/_{o}$) which is exactly the amount of excess water necessary for equivalent stiff slump. It is proposed that this improvement in packing efficiency from a dry mixture with the addition of water is related to the slump window, by producing the excess water content required for equivalent stiff slump.

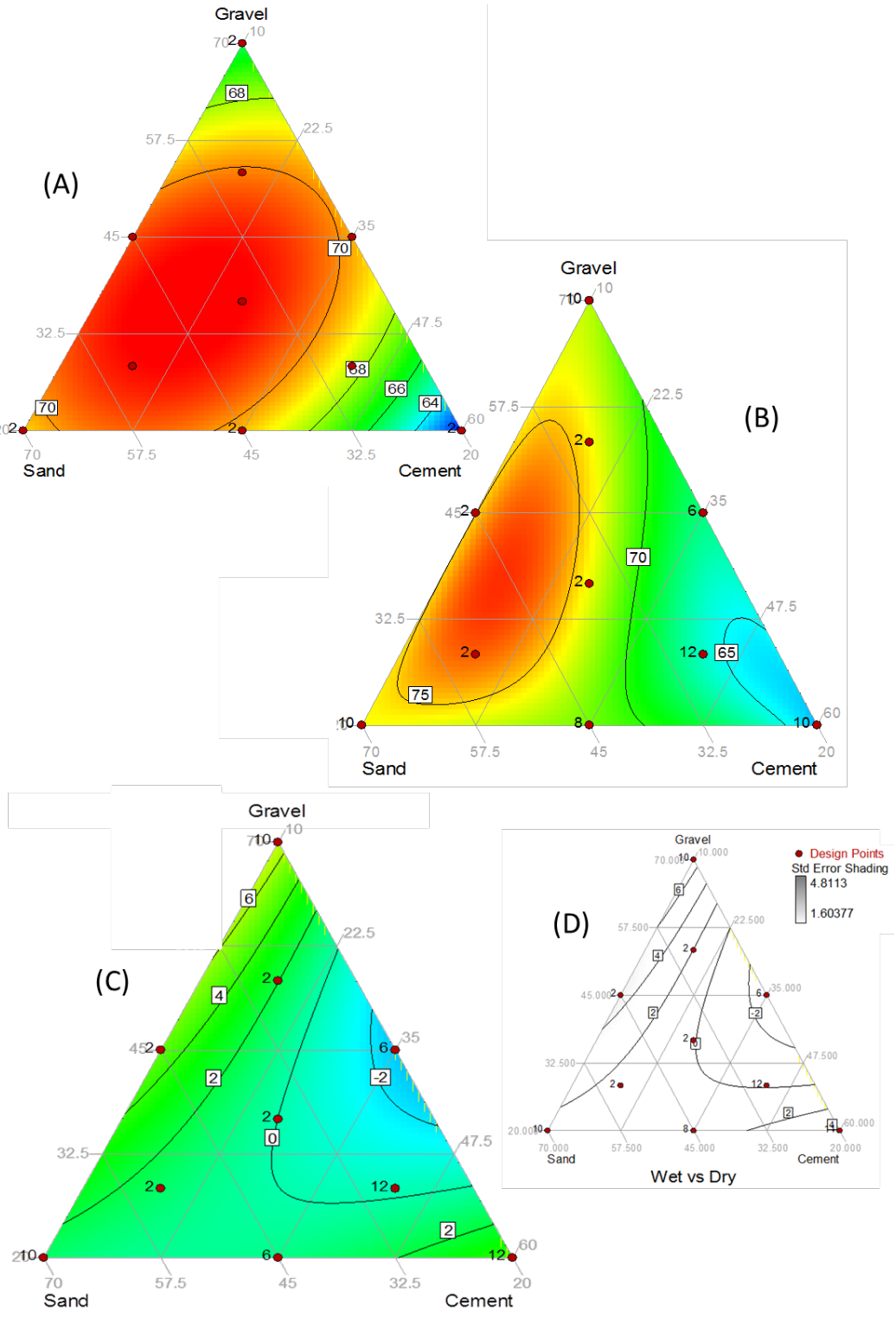

Figure 18. (A) The PE_D data extrapolated from full matrix, (B) The PE_W measured within the equivalent stiff slump region, (C) PE_W-PE_D within the slump matrix, (D) The standard error associated with (C).

The pore volume of the slump test decreased with tamping at each of the three tamping stages (as discussed in literature review). The tamping in the slump test reduces entrained air, while packing the material. The tap density process mimics the rodding technique. Entrained air reduces the packing efficiency. These results indicate a weak correlation between the level of entrained air (excess pore volume) and sand, as shown in Figure 19 (the dark line). Along this line – a 1:1 ratio of gravel to cement – the entrained air decreases with increasing sand. This trend appears to be valid over a range of gravel:cement ratios, spanning 60:40 to 40:60, but the correlation dissipates at higher gravel levels.

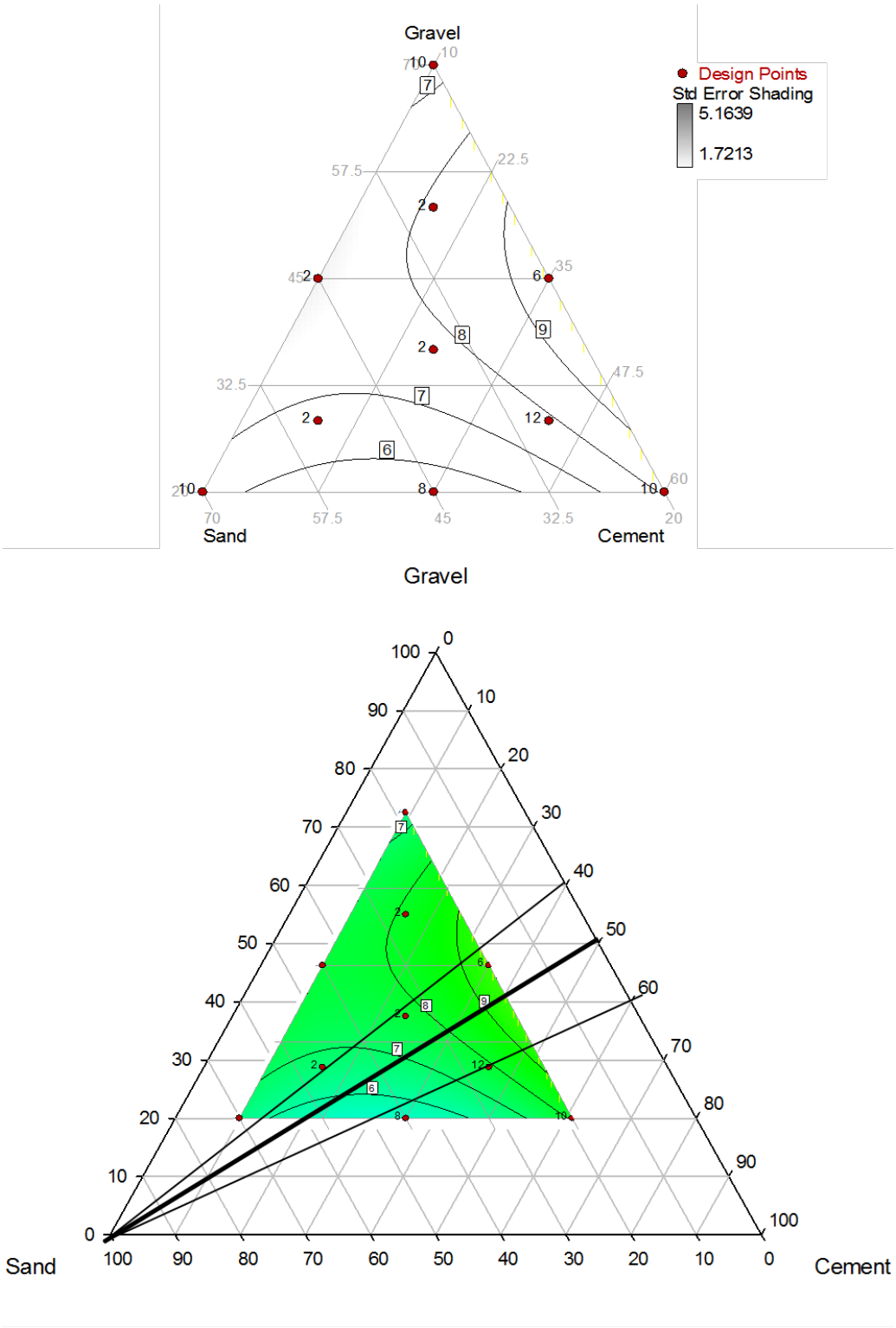

Figure 19. The pore volume displacement compared to the composition of sand within the slump testing matrix (below). The standard error ternary associated with the pore volume displacement.

B. Slump Testing

In forming methods such as extrusion, the excess water window for extrudability was determined to be 4-8 ($^{v}/_{o}$).[4] The determination of the slump "window" was based on the required excess water volume after correcting for the packing density increase observed with the addition of water. The standard states that the slump value must be rounded to the nearest 5th mm, which is the precision of the measurement.* Multiple trials of slump tests were measured and the results compiled in Figure 20. There is an obvious trend that slump increases with the addition of excess water. The relationship between slump and excess water is linear up to ~8 ($^{v}/_{o}$) excess water, where the relationship becomes nonlinear. Nonlinear equates to nonstandard slumps (shear, collapse, etc.) as presented in Figure 3.

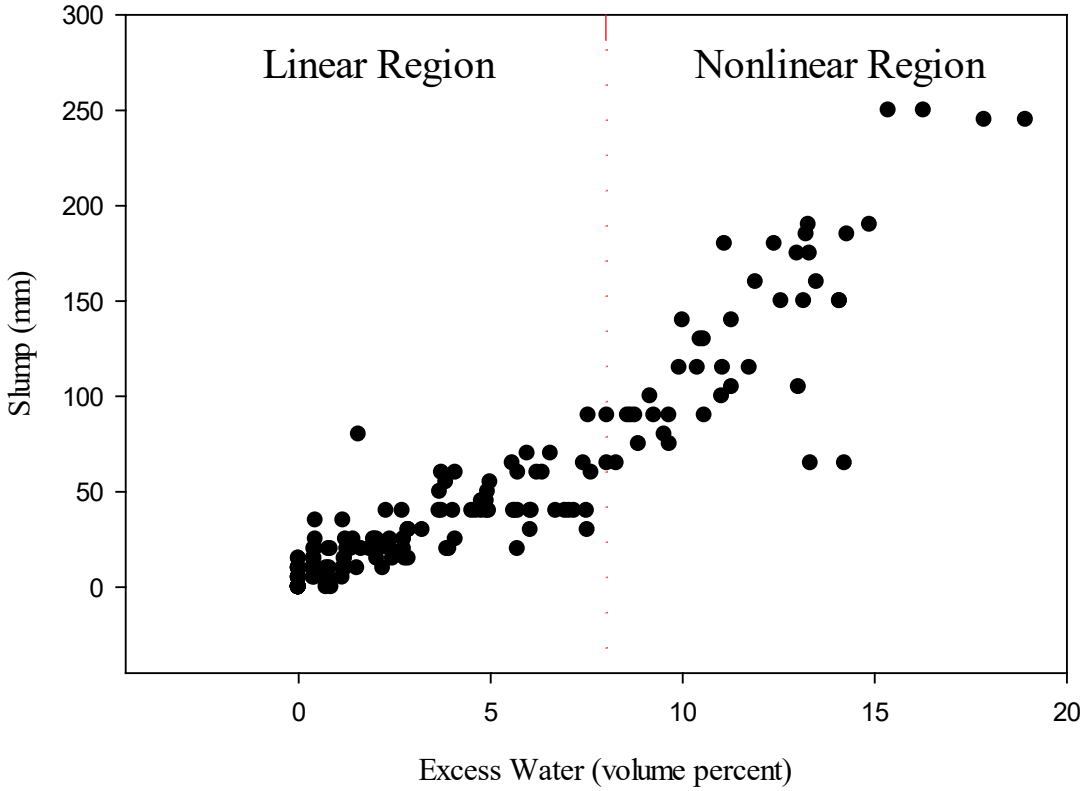

Figure 20. All slump data collected through the experiment separated at ~8 ($^{v}/_{o}$) as a linear region and nonlinear region.

* "Acceptable results of two properly conducted tests by the same operator on the same material will not differ from each other by more than the d2s (Acceptable Range of Two Results) value of the last column of Table 1 (Table III in this thesis) for the appropriate slump value and single-operator precision"[3]

A Shapiro-Wilks test P value of 0.7859 demonstrated that the excess water levels necessary for equivalent stiff slump were normally distributed. [21] Figure 21 shows a regression line which was used to determine the linear equation and the 95% confidence interval and prediction bands. Equation 9 could be used to calculate the slump (S) in millimeters, where (EW_X) is excess water in volume percent. The regression equation was determined to be:

$$S = 3.4 * EW_X + 17 \quad (9)$$

Figure 21 presents a significance level of 0.05. This figure could be used to help predict the excess water required for a specific slump or vice versa. The variability within the data was determined using the 95% prediction band for each composition. At a value of 3 ($^{v}/_{o}$) excess water, the slump within the prediction band is 12-42 mm slump, similar to the 15-45 mm level defined as equivalent stiff slump. The confidence interval is defined as the region comprised of the relationship of the true mean between the dependent and independent variables, when the prediction band also contains the sample number from where the observations were made.

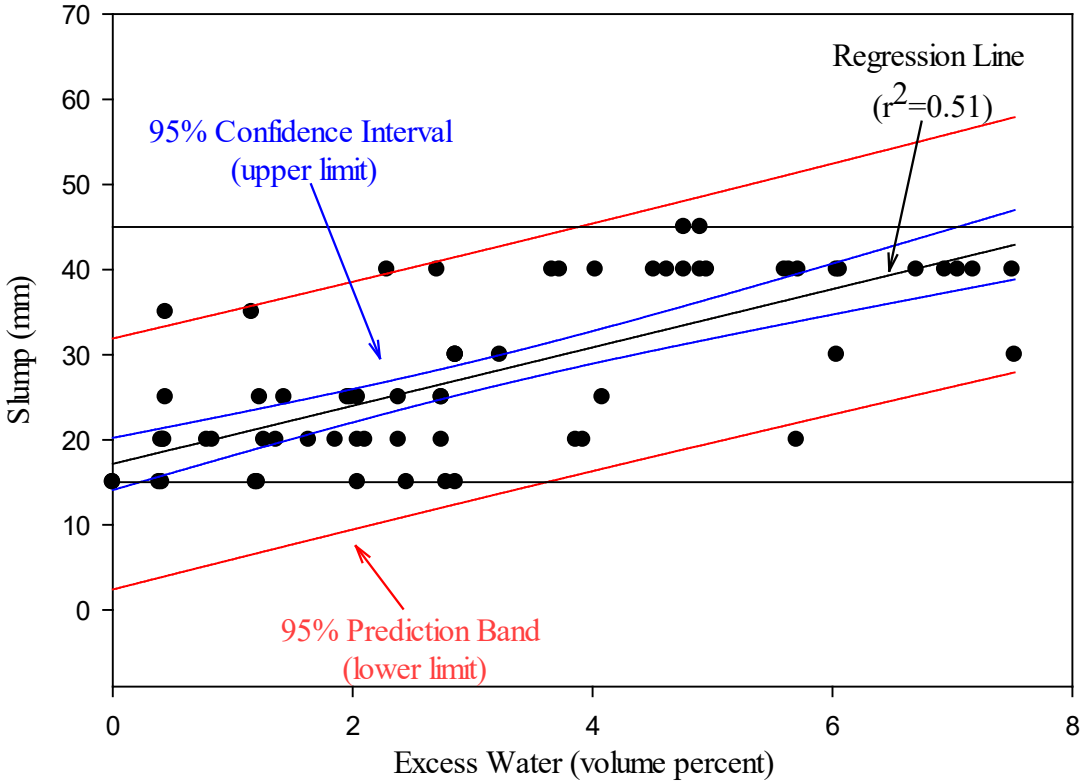

Figure 21. The slump values are compared to the excess water using a regression analysis with confidence intervals and a prediction band.

C. Excess Water Content Region

Figure 22 shows the relationship between excess water and packing efficiency. Excess water is independent of packing efficiency over the range of measured packing efficiencies (approximately 60%-80%). There was no clear trend of excess water level with overall composition, i.e., excess water amount did not appear to be sensitive to cement level (for example), as shown in Figure 23. The differences observed, ranging from 2-4 (%), are within the calculated standard deviation from the mean excess water level. The standard error over the entire experimental design space is less than one ($\frac{Standard\ Deviation}{\sqrt{Sample\ Size}}$).

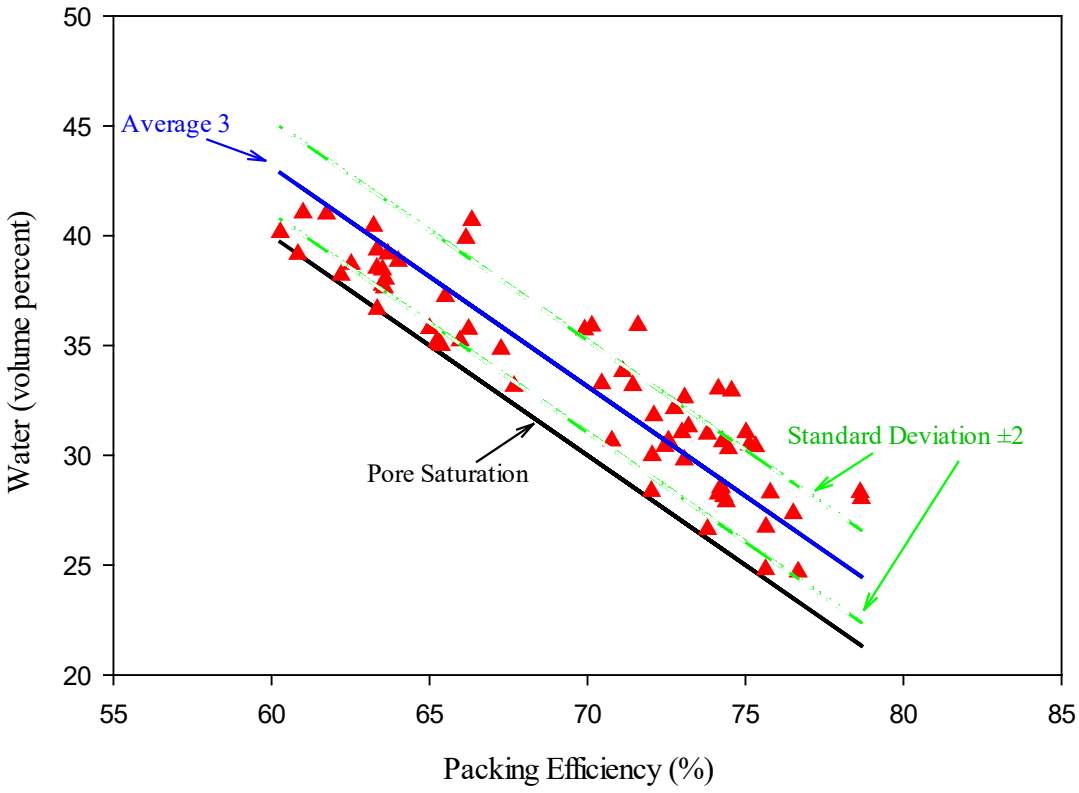

Figure 22. The pore saturation volume determined based on packing efficiency and the excess water content window calculated for equivalent stiff slump.

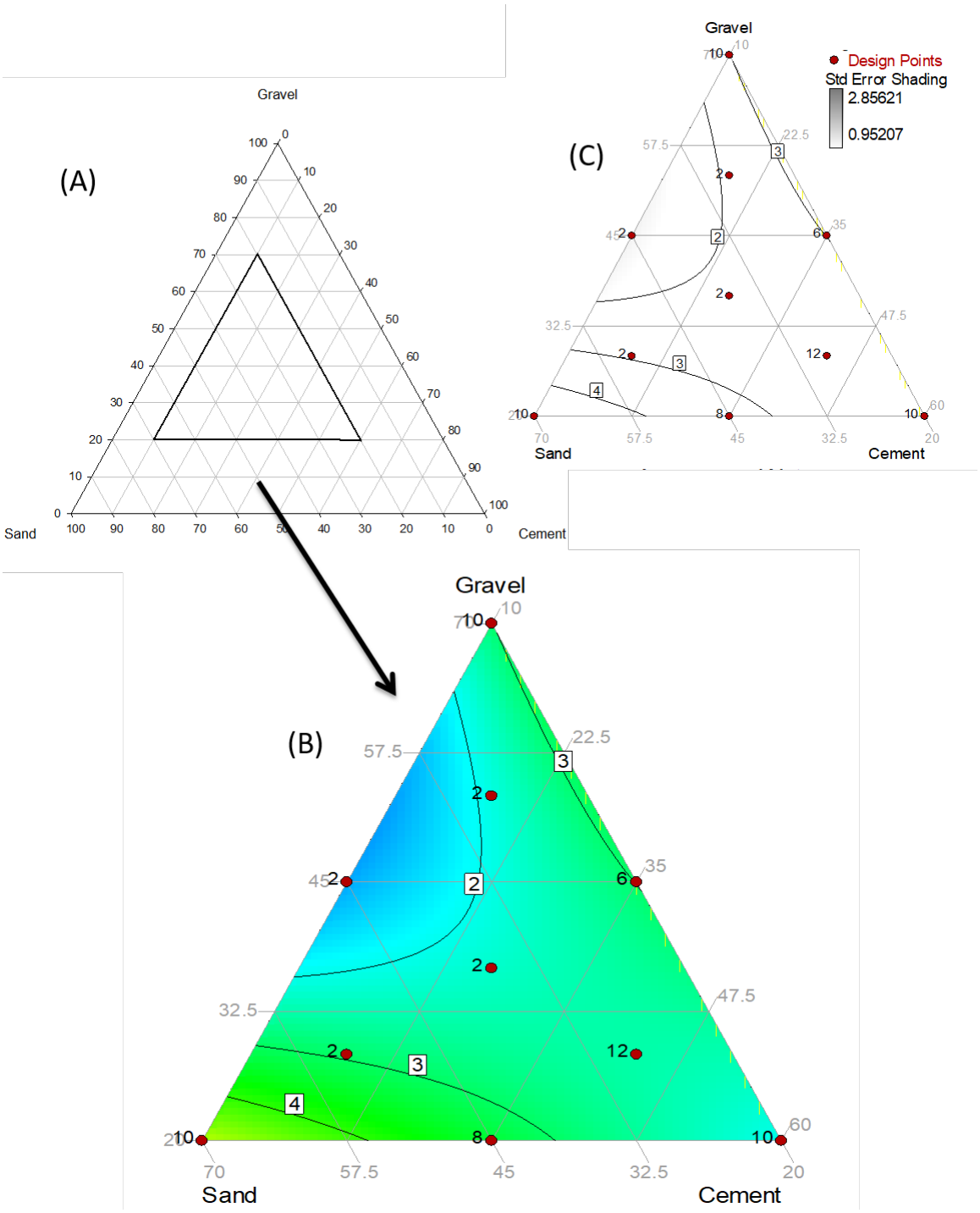

Figure 23. (A) The slumping location within the entire ternary plot. (B) The excess water that is required at each composition over the equivalent slump region of 15-45 mm. (C) The standard error ternary calculated from the excess water ternary diagram.

Figure 24 illustrates the excess water window for two packing efficiency levels (high and low) showing a constant excess water content window. The high packing efficiency (A) had a pore volume of 27% and low packing efficiency (B), had a pore volume of 37%. This figure illustrates that if the packing efficiency and density of the composition the excess water required for equivalent stiff slump can be determined.

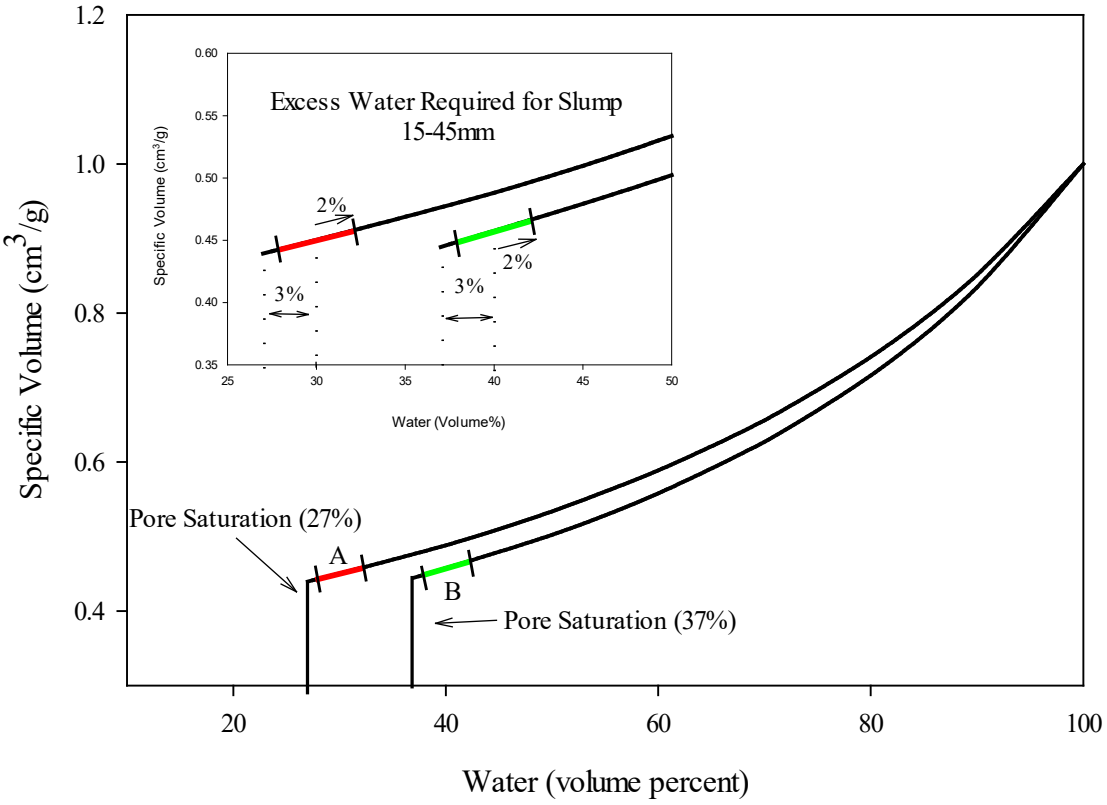

Figure 24. A specific volume diagram and excess water content window for composition 70:20:10 (A) and composition 20:20:60 (B). The excess water content window is 3±2 (%) for equivalent stiff slump.

D. Approaching The System As A Binary Mixture

Due to the overlap of the particle size and distribution of gravel and sand, it is proposed that this system could be more readily analyzed as a two component system composed of aggregate (gravel + sand) and cement rather than as a ternary. Figure 25 depicts the data representing a binary system by changing the gravel and sand ratio, over the cement content range of 10 ($^{v}/_{o}$) to 20 ($^{v}/_{o}$). Figure 26 uses the wet packing efficiencies to illustrate how the gravel and sand content affect the overall packing efficiency of the system. Table XI defines the packing efficiency region for 10 ($^{v}/_{o}$) and 20 ($^{v}/_{o}$) as 74±0.79 and 75±2.4 (statistically indistinguishable). Figure 14 defines the influence of cement on packing efficiency, which keeps the gravel and sand ratios constant at 1:1 (see Figure 13) but changing the ratio of gravel:sand does not significantly change the packing efficiency. The maximum packing efficiency occurs at approximately 82:18 (coarse:fine) ratio nearly identical to predicted ratio (80:20). Figure 27 brackets the range of possible particle sizes and distributions associated with the aggregate. The range for the samples that have been measured in the slump tests are between the upper gravel and sand limit presented in Figure 27. This 80:20 ratio is proposed to be valid if the coarse particle diameter follows the 10:1 ratio of the smaller particle. As previously discussed, Figure 9 illustrates the substantial overlap in the gravel and sand distribution which allows treatment as a binary system.

To transform this system into an ideal ternary mixture, the gravel would need to be coarser and the sand particle distribution would need to be narrowed to eliminate the overlap of the tails. By narrowing the sand distribution, the sand would achieve the necessary 10:1 size ratio with the cement. The benefit of a ternary system would be improved packing efficiency and lower water contents.

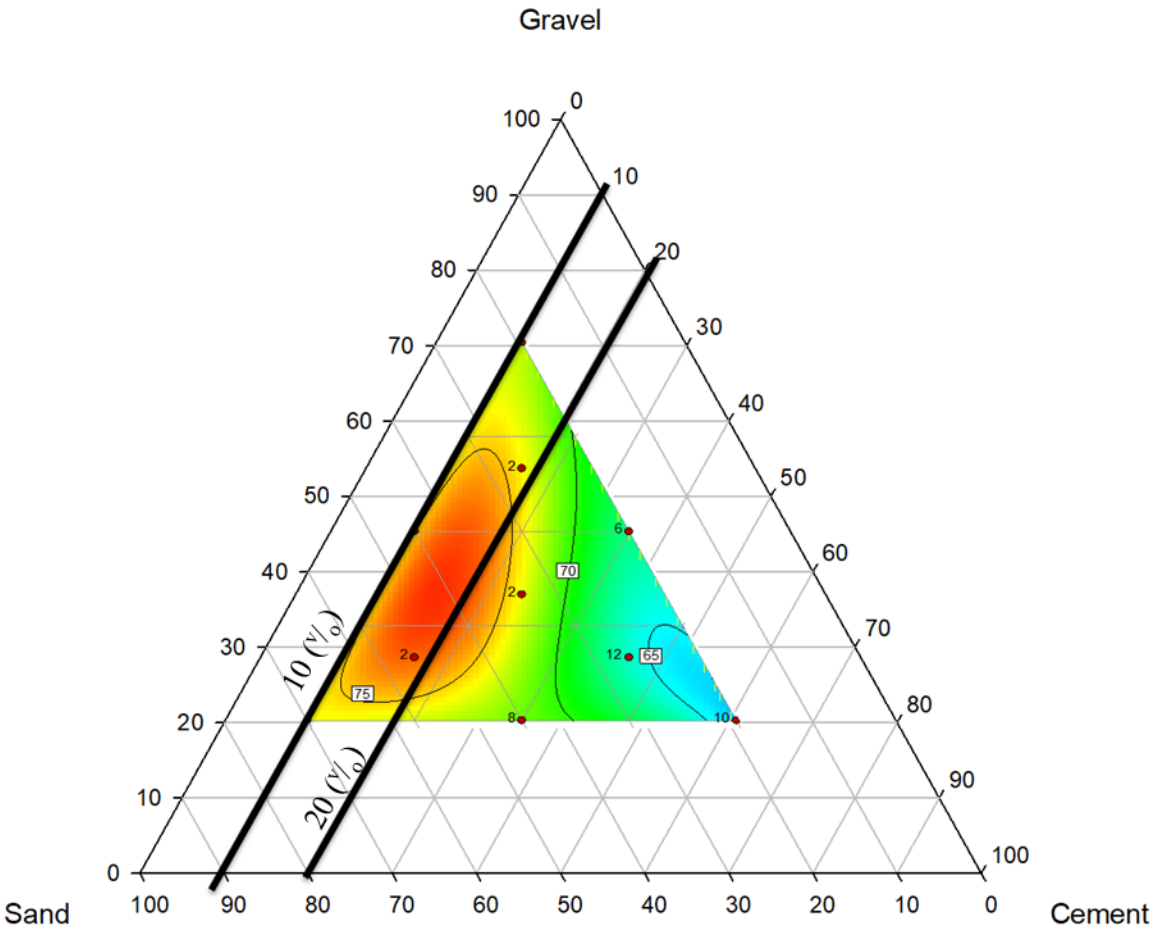

Figure 25. The wet packing efficiency over the area used for slump. The dark lines represent compositions with a constant 10 (v/o) and 20 (v/o) cement over a range of sand and gravel compositions.

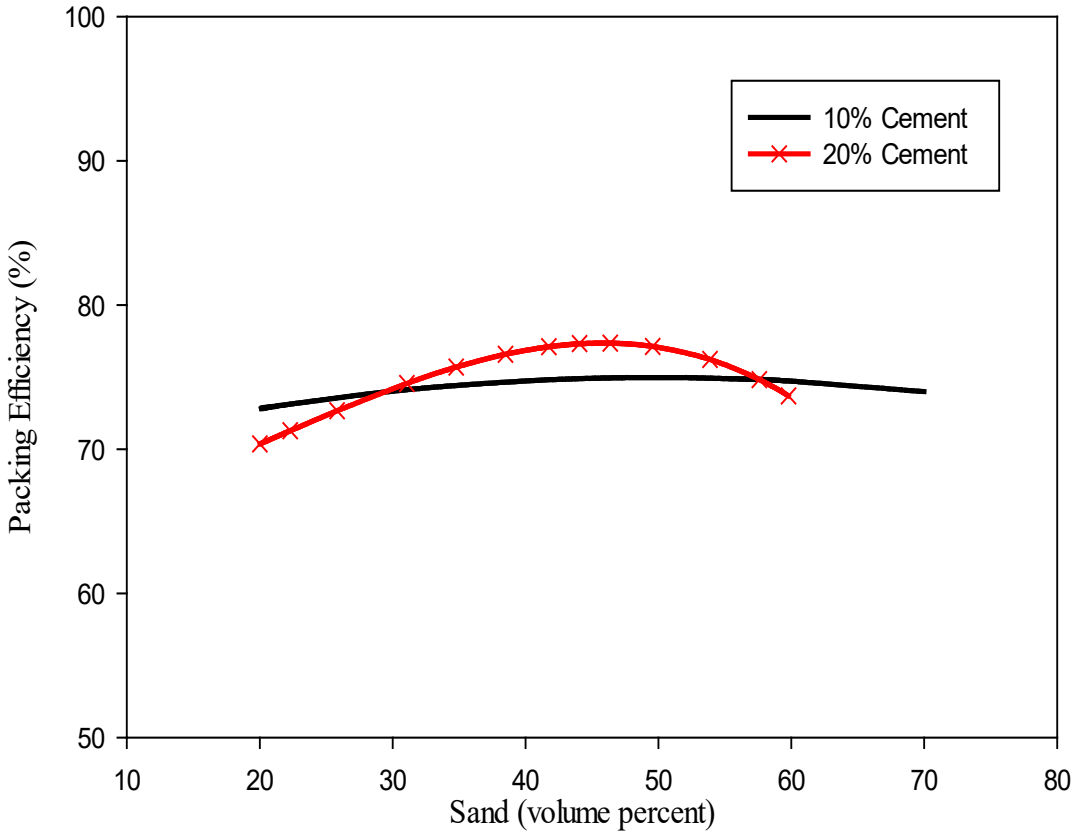

Figure 26. This is a two dimensional cross figure of the two dark lines in Figure 25. It represents the predicted wet packing efficiencies over a range of sand and gravel compositions while keeping a constant cement content of 10 (v/o) and 20 (v/o).

Table XI. The Average Packing Efficiency, Standard Deviation, and Packing Density Associated with Figure 26. Displaying the Differences Between the Constant Cement Content of 10 (v/o) and 20 (v/o).

Cement Content	**10 (v/o)**	**20 (v/o)**
Average Packing Efficiency (%)	74	75
Standard Deviation (%)	0.79	2.4
Packing Density (g/cm^3)	1.91 ±.01	2.05±.02

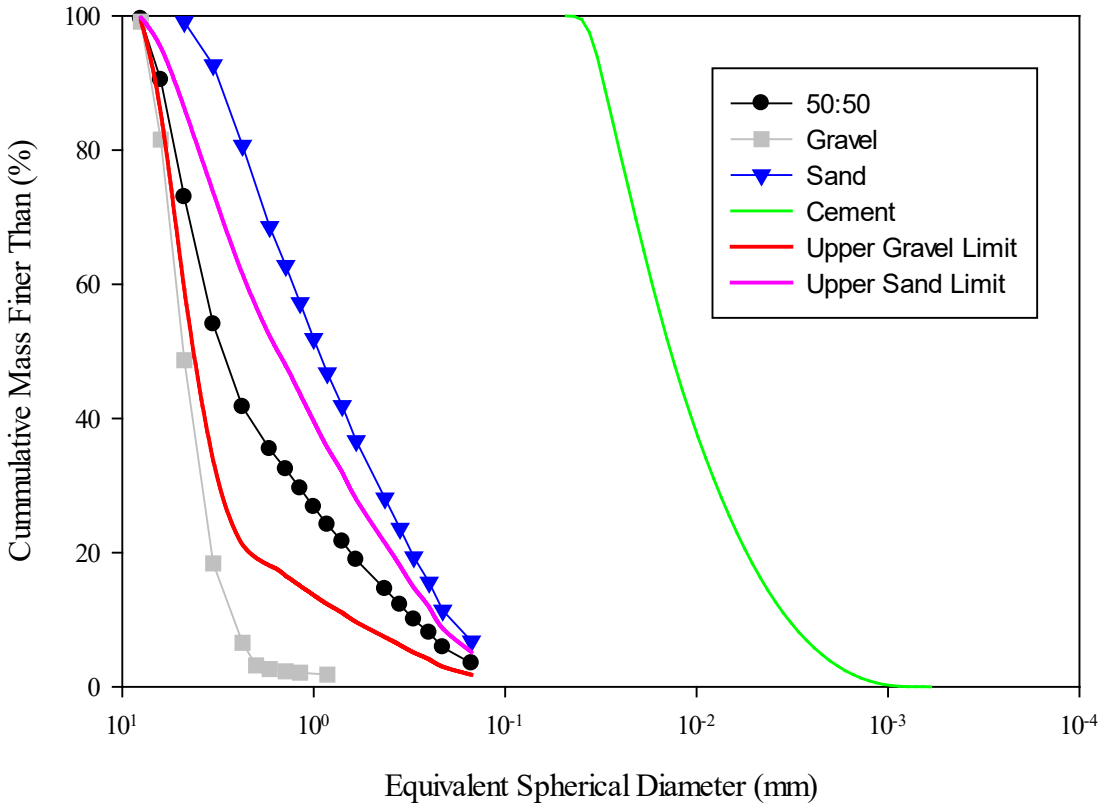

Figure 27. Particle size and distribution of gravel, sand and cement. Along with the particle size and distribution combining gravel and sand into one material with a ratio of 50:50. The upper gravel, and upper sand limits describe the wet packing efficiency ternary where gravel and sand are 90 ($^{v}/_{o}$) of the composition at a ratio of 70:20. The upper gravel limit has a ratio of 70:20 of gravel to sand while the upper sand limit is vice versa.

V. SUMMARY AND CONCLUSION

Concrete compositions are typically comprised of gravel, sand, and cement, and expressed in weight percent. A slump test is used to determine the flowability of the mixture, with water added to alter this consistency. In this work, a simple but new concept of using volume instead of weight percent for all constituents including water, allowed a better understanding of pore saturation and slump. Using a specific volume diagram approach, a constant window of 3 +- 2 v% excess water content was calculated for an equivalent stiff slump region. This is a significant result that can be further developed for use by the concrete industry to make decisions on water content required for a wide variety of starting materials in the equivalent stiff slump region of 15- 45 mm.

This work also demonstrated that the dry packing efficiency improved by 3 v% with the addition of sufficient water for pore saturation. Water in excess of pore saturation showed no effect on packing efficiency. It is proposed that the packing efficiency improvement is related to the excess water content window required for equivalent stiff slump. This improvement in packing efficiency is related to the slump window addition of water to a dry mixture, by producing the excess water content required for equivalent stiff slump. It is proposed that this improvement in packing efficiency from a dry mixture with the addition of water is related to the slump window, by producing the excess water content required for equivalent stiff slump.

A further conclusion of this thesis is that the concrete ternary system can effectively be treated as a binary system due to the overlap in particle size distribution of the gravel and sand. The packing efficiency of the system was not significantly altered as the cement was held constant, while the gravel and sand ratio's change. Simplifying the system as a combined aggregate (gravel + sand) plus cement generated optimum particle packing at a ratio of 82:18, equivalent to the predicted 80:20 from packing theory.

FUTURE WORK

The overlap of the particle size distributions creates a problem in the generation of well-packed systems. What is poorly understood is what level of overlap, or what fraction of the particle size distributions, can be below the required 10:1 size ratio before packing is adversely affected. To evaluate this, it is proposed that a series of carefully constructed, or scalped, distributions be generated and blended to systematically evaluate the role of particle size distribution overlap on packing behavior.

REFERENCES

1. G. C. Bye, *Portland Cement. Composition, Production and Properties*. The Institute of Ceramics, Reston, VA, 1983.

2. W. M. Carty, "Introduction to Ceramic Powder Processing," CEMS 203, Alfred University, Alfred, NY, 2016 (lecture notes).

3. "Standard Test Method for Slump of Hydraulic Cement Concrete," ASTM Designation C 143/143M-10. American Society for Testing and Materials, West Conshohocken, PA.

4. K. Bubb, "The Impact of Milled Alumina Particle Size and Distribution on Packing Efficiency and Paste Extrusion Pressures"; M.S. Thesis. Alfred University, Alfred, NY, 2016.

5. P. Ritt, "Implementation of Specific Volume Diagrams for Tape Casting"; B.S. Thesis. Alfred University, Alfred, NY, 2009.

6. J. Onofrio and G. Pomarico, "Determining the Excess Volume Window for Slump Behavior"; B.S. Thesis. Alfred University, Alfred, NY, 2017.

7. J. A. Ober, "Mineral Commodity Summaries 2016" (2016) USGS Science for a Changing World. Accessed on: March 2017. Available at <https://minerals.usgs.gov/minerals/pubs/commodity/cement/mcs-2016-cemen.pdf>

8. S. Popovics, *Concrete Materials. Properties, Specifications and Testing*, 2nd ed.; Noyes Publications, Park Ridge, NJ, 1992.

9. H. E. Davis and G. E. Troxell, *Composition and Properties of Concrete.* Edited by H. E. Davis. McGraw-Hill, New York, NY, 1956.

10. F.M. Lea, *The Chemistry of Cement and Concrete;* Chemical Publishing, New York, NY, 1971.

11. J. C. Walraven and S. Fennis, "Using Particle Packing Technology for Sustainable Concrete Mixture Design," *Heron Journal*, **57** [2] 73-102 (2012).

12. V. Zivica, "Effects of the Very Low Water/Cement Ratio," *Constr. Build. Mater.,* **23** [12] 3579-82 (2009).

13. A. K. H. Kwan and L.G. Li, "Packing Density of Concrete Mix under Dry and Wet Conditions," *Powder Technol.,* **253**, 514-21 (2014).

14. J. McCann, "Porcelain Aggregate in High-Strength Concrete"; M.S. Thesis. Alfred University, Alfred, NY, 2006.

15. G. Onoda Jr., "Specific Volume Diagrams for Ceramic Processing," *J. Am. Ceram. Soc*., **66** [4] 297-301 (1983).

16. S. S. Jamkar and M. N. Mangulkar, "Review of Particle Packing Theories Used for Concrete Mix Proportioning," *Int. J. Sci. Eng. Res*., **4** [5] 143-48 (2013).

17. R. K. McGeary, "Mechanical Packing of Spherical Particles," *J. Am. Ceram. Soc*., **44** [10] 513-22 (1961).

18. H. M. Jennings, A. W. Saak, and S. P. Shah, "A Generalized Approach for the Determination of Yield Stress by Slump and Slump Flow," *Cem. Concr. Res,* **34** [3] 363-71 (2004).

19. "Slump Test" (2010). Accessed on: April 2017. Available at <http://civil-online2010.blogspot.com/2010/02/slump-test.html>

20. "Standard Test Method for Sieve Analysis of Fine and Coarse Aggregates," ASTM Designation C 146/C136M-14. American Society for Testing and Materials, West Conshohocken, PA.

21. W. Mendenhall and T. Sincich, *Statistics For Engineering And The Sciences*, 3rd ed. Macmillan Publishing Company, New York, NY, 1992.

APPENDIX

A. Designs 1-6 for Dry Packing Efficiencies. Duplicate Numbers Indicate Replicants.

Design 1

Standard Order	Run Order	Gravel	Sand	Cement	Packing Efficiency
1	1,2	80	15	5	60.9, 60.8
2	10,13	65	30	5	73.4,73.5
3	4,14	65	15	20	69.3, 67.8
4	7,11	72.5	22.5	5	61.9, 64.0
5	8	72.5	15	12.5	64.9
6	5	65	22.5	12.5	67.8
7	6	75	17.5	7.5	64.0
8	9	67.5	17.5	15	67.3
9	12	67.5	25	7.5	65.0
10	3	70	20	10	65.6

Design 2

Standard Order	Run Order	Gravel	Sand	Cement	Packing Efficiency
1	5,12	70	20	10	66.0, 66.1
2	3,13	55	35	10	67.6, 66.3
3	2,9	55	20	25	69.9, 70.8
4	1,7	62.5	27.5	10	65.6, 67.9
5	4	62.5	20	17.5	71.2
6	10	55	27.5	17.5	69.6
7	14	65	22.5	12.5	66.6
8	6	57.5	30	12.5	69.3
9	8	57.5	22.5	20	68.7
10	11	60	25	15	67.7

Design 3

Standard Order	Run Order	Gravel	Sand	Cement	Packing Efficiency
1	10,13	75	10	15	62.5, 63.3
2	2,9	60	25	15	69.5, 71.5
3	3,7	60	10	30	68.5, 68.8
4	1,14	67.5	17.5	15	68.3, 67.5
5	4	67.5	10	22.5	65.7
6	12	62.5	12.5	25	71.0
7	5	70	12.5	17.5	68.7
8	8	62.5	20	17.5	69.6
9	11	60	17.5	22.5	71.4
10	6	65	15	20	69.4

Design 4

Standard Order	Run Order	Gravel	Sand	Cement	Packing Efficiency
1	2,9	50	40	10	69.4, 70.3
2	1,13	20	70	10	69.4, 72.4
3	7,14	20	40	40	64.9, 65.0
4	5,6	35	40	25	72.9, 71.9
5	11	35	55	10	71.8
6	3	20	55	25	72.4
7	4	40	45	15	73.5
8	8	25	60	15	75.7
9	10	25	45	30	69.4
10	12	30	50	20	73.5

Design 5

Standard Order	Run Order	Gravel	Sand	Cement	Packing Efficiency
1	3,8	100	0	0	55.6, 55.6
2	5,7	0	100	0	65.4, 65.4
3	2,10	0	0	100	42.2, 42,2
4	1,14	50	50	0	67.0, 65.8
5	13	50	0	50	60.2
6	12	0	50	50	61.7
7	11	66.6	16.6	16.6	67.5
8	4	16.6	66.6	16.6	74.6
9	9	16.6	16.6	66.6	53.7
10	6	33.3	33.3	33.3	68.2

Design 6

Standard Order	Run Order	Gravel	Sand	Cement	Packing Efficiency
1	13,14	70	10	20	71.8, 69.8
2	3,7	45	35	20	73.4, 73.5
3	4,9	45	10	45	65.0, 65.6
4	1,12	57.5	22.5	20	70.2, 73.0
5	10	57.5	10	32.5	71.4
6	5	45	22.5	32.5	71.3
7	8	61.6	14.2	24.2	71.6
8	6	49.2	26.6	24.2	72.7
9	2	49.2	14.2	36.6	67.8
10	11	53.3	18.3	28.3	71.0